DEPARTMENT OF PHYSICS, UNIVERSITY OF JYVÄSKYLÄ

RESEARCH REPORT No. 9/2000

Small Normal–metal Tunnel Junctions in Electromagnetic Environment

BY

SHADYAR FARHANGFAR

Academic Dissertation

for the Degree of

Doctor of Philosophy

Jyväskylä, Finland

November 2000

URN:ISBN:978-951-39-9451-8
ISBN 978-951-39-9451-8 (PDF)
ISSN 0075-465X

Jyväskylän yliopisto, 2022

ISBN 951-39-0821-6
ISSN 0075-465X

DEPARTMENT OF PHYSICS, UNIVERSITY OF JYVÄSKYLÄ

RESEARCH REPORT No. 9/2000

SMALL NORMAL–METAL TUNNEL JUNCTIONS IN ELECTROMAGNETIC ENVIRONMENT

BY

SHADYAR FARHANGFAR

Academic Dissertation

for the Degree of

Doctor of Philosophy

To be presented, by permission of the

Faculty of Mathematics and Science

of the University of Jyväskylä,

for public Examination in Auditorium FYS 1 of the

University of Jyväskylä on December 8, 2000,

at 12 o'clock noon

Jyväskylä, Finland

November 2000

CONTENTS

Preface 4

Abstract 5

List of Publications 7

The Author's Contribution 8

OVERVIEW OF SINGLE ELECTRONICS 9

1.1 Introduction 9

1.2 Tunneling 11

1.3 The Coulomb Blockade 12

THEORETICAL CONSIDERATIONS 14

2.1 The Weak Tunneling Regime 14

2.2 The Monte-Carlo Simulations 23

2.3 The Strong Tunneling Regime 25

2.3.1 The Extended Phase-correlation Theory 25

2.3.2 The Path-integral Method 27

2.3.3 The Quasiclassical Langevin Equation Approach 30

2.4 The Voltage Fluctuations Model 39

RESULTS AND CONCLUSIONS 41

3.1 Review of the Basic Results in the Weak Tunneling Regime 41

3.2 Single Tunnel Junctions 42

3.3 Tunnel Junction Arrays 50

3.3.1 One-dimensional Arrays of Low-conductance Tunnel Junctions . . . 51

3.3.2 One-dimensional Arrays of High-conductance Tunnel Junctions . . . 53

3.3.3 Two-dimensional Arrays of Tunnel Junctions 61

EXPERIMENTAL TECHNIQUES 69

A.1 Sample Fabrication 69

A.2 Cooling of the Samples 71

A.3 Measuring Electronics 71

References **74**

PREFACE

In my thesis, I will first have an overall look on the subject of *Single Charge Tunneling*: where it comes from and why it is of interest. After introducing the necessary concepts and tools, I will give a review of what had already been done before the starting of this project. Finally, the main results of this thesis will be discussed. In all the stages of the text, my goal has been to stress the points which, even trivial to some people, have not been completely clear to me. If one is only seeking for the main results and does not get satisfaction with, or could not be bothered to read, down-to-earth presentations, he/she can skip this part and start with the abstracts of the articles attached.

I wish to thank my teacher and supervisor, Academy Professor, Jukka Pekola.

Jyväskylä, November 2000

SHADYAR FARHANGFAR

ABSTRACT

The effect of the electromagnetic environment on single junctions and on one– and two–dimensional arrays of junctions has been studied theoretically. The phase–correlation theory [or the $P(E)$ theory], originally developed for the weak tunneling regime, its extension to the regime of strong tunneling, and the quasiclassical Langevin equation model have been investigated in more detail. The path–integral method and the voltage fluctuations model are shortly introduced. Limitations of each model along with its domain of applicability have also been discussed.

The main results of the phase–correlation theory in the high temperature limit, *i.e.* for junctions with the Coulomb gap smaller than the thermal energy $k_{\mathrm{B}}T$, are reviewed. While doing this, emphasis has been put on the Coulomb blockade thermometry (CBT) applications. Results have been earlier obtained for the case of negligible environmental impedance. Here, the effect of the electromagnetic environment is investigated both theoretically and experimentally. This is done first for the single tunnel junctions, then for the one–dimensional (1D) and finally for two–dimensional (2D) arrays of tunnel junctions.

It is shown that the effect of the electromagnetic environment is most pronounced for solitary tunnel junctions and, as another important example for two–junction arrays, and becomes negligible by increasing the number of junctions in an array. Furthermore, the strong tunneling corrections to the basic phase–correlation theory improve the agreement between the theory and our measurements in the case of solitary tunnel junctions with resistances much smaller than the quantum resistance $R_{\mathrm{K}} \simeq 25.8$ kΩ. Performing the Monte–Carlo simulations for arrays of tunnel junctions with $N \geq 2$, we show that there is a value of external electromagnetic impedance, typically ~ 0.5 kΩ, at which the half–width of the conductance curve around zero bias voltage, $V_{1/2}$, shows a maximum. This observation is further confirmed by the measured data, although the quantitative agreement is only fair.

Introducing a relatively simple theory for the high–conductance 1D arrays, *i.e.* for arrays in the strong tunneling regime, the measured data for these structures together with their comparison to the theoretical predictions are presented. This is done with an eye on CBT

applications. The desired strong tunneling correction to the simple linear relation used in the thermometry, $V_{1/2,0} = 5.439Nk_{\mathrm{B}}T/e$, is given. The effect of non–homogeneity of tunnel junctions on the tunneling in the arrays has been discussed, as well.

In the last part, assuming that the tunneling regime is sequential, the $P(E)$ theory has been applied to the topologically simple two–dimensional structures. The results have been compared to the measured data, and it has been shown that, as thermometers, 1D arrays are superior to their 2D counterparts.

PACS. 73.23.Hk — Coulomb blockade; single–electron tunneling.

PACS. 73.40.Gk — Tunneling.

PACS. 73.40.Rw — Metal–insulator structures.

LIST OF PUBLICATIONS

The main results of this thesis have already been published ([P1]–[P4]) or accepted for publication ([P5]):

[**P1**] *One–dimensional arrays and solitary tunnel junctions in the weak Coulomb blockade regime: CBT thermometry*, Sh. Farhangfar, K. P. Hirvi, J. P. Kauppinen, J. P. Pekola, D. V. Averin, and A. N. Korotkov, J. Low Temp. Phys. **108**, 191 (1997).
https://doi. org/10. 1007/BF02396821

[**P2**] *Experiments on tunneling in small normal–metal tunnel junctions influenced by dissipative environment: Critical comparison to the theories of quantum fluctuations*, Sh. Farhangfar, J. J. Toppari, Yu. A. Pashkin, A. J. Manninen, and J. P. Pekola, Europhys. Lett. **43**, 59 (1998).
https://doi. org/10. 1209/epl/i1998-00319-x

[**P3**] *Effect of the electromagnetic environment on arrays of small normal–metal tunnel junctions: Numerical and experimental investigation*, Sh. Farhangfar, A. J. Manninen, and J. P. Pekola, Europhys. Lett. **49**, 237 (2000).
https://doi. org/10. 1209/epl/i2000-00139-0

[**P4**] *One– and two–dimensional tunnel junction arrays in weak Coulomb blockade regime —absolute accuracy in thermometry*, J. P. Pekola, L. J. Taskinen, and Sh. Farhangfar, Appl. Phys. Lett. **76**, 3747 (2000).
https://doi. org/10. 1063/1. 126770

[**P5**] *Coulomb blockade in one–dimensional arrays of high–conductance tunnel junctions*, Sh. Farhangfar, R. S. Poikolainen, J. P. Pekola, D. S. Golubev, and A. D. Zaikin, to appear in Phys. Rev. B (Feb. 15, 2001).
https://doi. org/10. 1103/PhysRevB. 63. 075309

THE AUTHOR'S CONTRIBUTION

I have fabricated, measured and analyzed the solitary tunnel junction samples of the first publication, [P1]. Most of the samples of [P2] were made, measured and analyzed by me. In addition, I contributed to the writing of this Letter. All the samples in the third publication, [P3], were made, measured and analyzed by the author. The Monte–Carlo simulations involved in this Letter were further developed and performed by me. This publication was also written by me. In [P4], I participated in the data analysis, made the theoretical calculations, and wrote parts of the Letter. In [P5], I took part in the data analysis and wrote the experimental part of the paper.

Chapter 1:

OVERVIEW OF SINGLE ELECTRONICS

1.1 Introduction

Since the invention of a solid state transistor in 1947, attempts have been made to benefit the properties of these materials in more and more applications. This has several advantages: speeding up the operation of the devices, saving in construction materials and consequently protecting the ecological environment, making the devices lighter in weight, and reducing the size of the components. During the last decades, progress in approaching these goals has been enormous, and probably one of the most influential ones in the history of science and technology. Nowadays, many of us have the privilege to taste the fruits of such advancement. While writing this thesis, the author of these lines is sitting in front of a sympathetic laptop computer by which many of the numerical calculations of this work, major part of the data analysis, and many other things related are being performed. This is impressive, and even beyond the imagination of some of the scientists of our era who passed away not very long time ago.

But, how much longer is the progress going to last? Is it possible to proceed forever using only the well established conventional methods? And, if not, how can one surpass this obstacle? The answer to the former question is a strict "no". And, the reason for this is the minimum theoretical line–width achievable by the *Optical Lithography* techniques. This line–width cannot be by orders narrower than the wavelength of the visible light ($\sim$ 300 nm) used in the imaging process. So, one should use a *beam* with a narrower wavelength. A good candidate to this end are electrons. By the laws of nature and as a consequence of

their subatomic size, electrons own wave-like properties, and therefore, a beam of coherent electrons with a specific energy, should have a characteristic wavelength. Since electrons could have wavelengths smaller than that of visible light, and this is, ultimately, what we are seeking for. The technique which puts this property of electrons to use for the imaging process is called *Electron Beam Lithography* (*EBL*), and nowadays it is one of the main tools for fabricating controlled submicrometer sized structures.

Knowing a way to make very "small" structures, our ultimate goal, as in the conventional electronic industry nowadays, is to make tiny components, and finally very small, and fast, integrated circuits (IC) with desired operational features.† Here, once again, one will use different materials, *i.e.*, metals, semiconductors and insulators. However, there *is* a difference which makes life harder —at least at first sight. Our components start to behave strangely. This can be a consequence of change in the bulk properties of the materials used on submicron scales, and/or a result of a chain of physical phenomena inside the component. Some of these peculiarities are material-dependent, while the others are not. An example of the first category is the phenomenon of *Superconductivity*. This happens for a class of materials at different temperatures. And, as an example for the latter category, one may mention the *Coulomb Blockade* effect. The second phenomenon constitutes the conceptual cornerstone of the field called *Single Charge Tunneling*. Contrary to the case with superconductivity, Coulomb blockade was first predicted by a very simple theoretical deduction and was observed only a few years later in 1987 by Fulton and Dolan [2]. Coulomb blockade will be presented after a review of the phenomenon of tunneling.

---

† The importance of progress in making components tiny and fast has now been crowned by awarding the year 2000 Nobel Prize to people working in the related fields: J. S. Kilby received half of the prize "for his part in the invention of the integrated circuit". The other half was jointly awarded to H. Kroemer "for developing semiconductor heterostuctures used in high–speed- and opto–electronics" and to Z. I. Alferov "for basic work on information and communication technology".

1.2 Tunneling

Tunneling has been known since the early days of quantum mechanics. Whenever a subatomic particle penetrates through a classically forbidden region, *barrier*, one speaks about tunneling. This energetically forbidden region can have a real physical counterpart, like the tunnel barrier of a tunnel junction consisting of two conducting parts separated by an insulator, or it can be without any concrete physical counterpart, as it happens inside the atomic nuclei in respect with the alpha decay.

A *tunnel junction* consists of two conductors separated by an insulator. In this work, typically, aluminum films have been used to make the conducting parts, and aluminum oxide to make the barrier. Depending on the temperature, the junction can be made superconducting or normal. It is also possible to fabricate the conducting parts of a tunnel junction of different materials.

Classically, the tunnel junction is a plate capacitor. Knowing the capacitance (which can be estimated by different methods), size of the plates, and using the simple classical relation for the plate capacitor, one finds that the thickness of the insulator layer is of the order of ten ångstroms. It is in such a thin layer that it would not be completely surprising if one observes some effects which could not be understood classically. As an example, one can mention the finite net electrical current passing through a tunnel junction if its leads are connected to a voltage source. This is simply a consequence of the electron tunneling through a barrier. Another quantum mechanical effect which is in close connection with the tunneling effect is the existence of negative differential resistance in solid state rectifiers (diodes). Leo Esaki was the first who explained this phenomenon and later, thanks to this, shared the Nobel prize of 1973 with Brian Josephson (for prediction of the effects in superconducting tunneling called after him) and Ivar Giaver (for the observation of the superconducting energy gap).

Contrary to the above–mentioned phenomena which can be understood by the simple *semiconductor model*, there are less "trivial" phenomena, like the *dc–* and the *ac–Josephson effects*. The dc–Josephson effect predicts the existence of a finite current at zero bias voltage in a superconducting *weak link* (like a superconducting tunnel junction), whereas according

to the ac–Josephson effect, a finite *direct* voltage difference across the leads would produce an *alternating* current with predicted frequency passing through the system. Nowadays, the ac–Josephson effect has various uses in metrology and devices employing this effect have found their way even to medical sciences.

1.3 The Coulomb Blockade

As a classical capacitor, the typical capacitance of a tunnel junction, C, made by electron beam lithography techniques is in the range of one femtofarad (10^{-15} F). Now, supposing that the initial electric charge on such a capacitor is Q, let us investigate what happens if this charge is changed by the charge of one single electron, *i.e.* by a charge $e \simeq -1.6 \times 10^{-19}$ C.[†]

The very basic condition for such an event is the favorableness of energy change in the system, namely, the change in the charging energy, $\delta E_{\rm C}$, should be positive:

$$\delta E_{\rm C} \equiv \frac{Q^2}{2C} - \frac{(Q \pm e)^2}{2C} > 0, \tag{1}$$

or $\mid Q \mid > e/2$, implying that the voltage difference across the junction should be greater than $e/2C$. At voltages smaller than this, the *one by one* (or *sequential*) tunneling of single electrons is forbidden. This, in turn, means the blockade of "single electron current" through the junction. This central phenomenon of the present thesis is called *Coulomb blockade*.

With typical values of the junction capacitances (0.1 fF$\lesssim C \lesssim$1 fF), the charging energy of the junction can be estimated to be in the range of 10^{-5}eV$\lesssim E_{\rm C} \lesssim 10^{-4}$ eV. This is comparable to the superconducting energy gap, $\Delta_{\rm g}$, of aluminum (2×10^{-4} eV) and its observation, as discussed above, presumes temperatures below that of liquid helium ($T \lesssim 4.2$ K).

[†] The total charge on the capacitor, Q, is a *continuous* variable, whereas here one is interested in *quantized changes* of this charge, that is, ne, where n is an integer number. The total charge, Q, is of the so-called *polarized* type, because it is a combined consequence of the polarization of *ions* on the capacitor plates *and* cloud of *electrons* there, whereas the change in that, ΔQ, *may* be quantized, as a consequence of, for instance, tunneling of single electrons [1].

It is worth–noticing that in the case of a superconducting tunnel junction, a similar argumentation for the tunneling of Cooper pairs can be done. Here, one simply substitudes the electron charge, e, by its superconducting counterpart $2e$. This, however, does not influence the order-of-magnitude argumentation presented above, which means that in a superconducting tunnel junction charging effects may compete with those arising from the superconductivity of the system.

In Chapter 2, the basic machinery for the description of single charge tunneling effects will be introduced. Starting with the results of basic *Orthodox Theory*, the well established *Phase–correlation Theory* (originally developed for the so-called *Weak Tunneling* regime) will be presented, followed by its extensions to the regime of *Strong Tunneling*. The *Path–integral Method*, applicable to ***both*** the weak and the strong tunneling regimes, will be shortly discussed in the context of our goals. The *Quasiclassical Langevin Equation Approach* will be discussed in more details. The reason is that, despite its relative simplicity, it is very efficient in the description of high–conductance tunnel junctions. The *Voltage Fluctuations Model* will only be shortly presented, since this model fails to be competitive with the existing microscopic theories. In Chapter 3, the main experimental results of this thesis together with their comparison to the theoretical predictions will be discussed.

Chapter 2:

THEORETICAL CONSIDERATIONS

2.1 The Weak Tunneling Regime

Since a major part of the phenomena studied in this thesis arise from the tunneling of single charges, one should evaluate the *tunneling rates*, Γ, of these events. To do this, let us start with the simplest case of a single tunnel junction without any explicit electromagnetic environment. We suppose that this junction is coupled to a perfectly biased voltage source [Fig. 1 (a)]. In a tunneling event the number of single charges on the plates of the junction changes. This, in turn, changes the charging energy of the system by the amount δE_{C}. The forward (backward) tunneling rate, $\Gamma^{(+)}_{(-)}$, can now be evaluated, and the result, according to the orthodox theory [3], is:

$$\Gamma^{\pm} \equiv \Gamma(\pm\delta E_{\mathrm{C}}) = \frac{1}{e^2 R_{\mathrm{T}}} \frac{\mp\delta E_{\mathrm{C}}}{1 - \exp(\pm\delta E_{\mathrm{C}}/k_{\mathrm{B}}T)}. \tag{2}$$

Here, R_{T} is the resistance of tunnel junction at large bias voltages. For a double–junction array [Fig. 1 (b)], the corresponding expression is quite similar, but here in addition to the *electrostatic energy change* of the j-th junction, $\delta F_j^{\pm}$, the tunneling rates depend on the number of *excess* charges, n, on the *island* connecting the two junctions:

$$\Gamma_j^{\pm}(n) \equiv \Gamma\left(\delta F_j^{\pm}(n)\right) = \frac{1}{e^2 R_{\mathrm{T}}} \frac{-\delta F_j^{\pm}}{1 - \exp(\delta F_j^{\pm}/k_{\mathrm{B}}T)}. \tag{3}$$

Extension of the above result to the case of an N–junction array [Fig. 1 (c)] is straightforward:

$$\Gamma_j^{\pm}(\{n\}) \equiv \Gamma\left(\delta F_j^{\pm}(\{n\})\right) = \frac{1}{e^2 R_{\mathrm{T}}} \frac{-\delta F_j^{\pm}}{1 - \exp(\delta F_j^{\pm}/k_{\mathrm{B}}T)}, \tag{4}$$

where $\{n\} \equiv \{n_1, n_2, \ldots, n_{N-1}\}$ designates the *charge configuration* on the islands and

$$\delta F_j^{\pm} \equiv \frac{q}{2}\left\{(\phi_{j\pm1} + \phi'_{j\pm1}) - (\phi_j + \phi'_j)\right\}. \tag{5}$$

Above, $\phi \equiv \phi(\{n\})$ and $\phi' \equiv \phi(\{n'\})$ indicate the electric potential of the electrodes before and after tunneling, respectively, and q is the electric charge of the tunneling particle (e or $2e$). In the stationary state, the current passing through the different junctions is the same, $I_1 = I_2 = \cdots = I_N$, and one can write

$$I \equiv I_k = e \sum_{\{n\}} \sigma(\{n\}) \left[\Gamma_k^+(\{n\}) - \Gamma_k^-(\{n\})\right]. \tag{6}$$

Here, $\sigma(\{n\})$ is the probability for the charge configuration $\{n\}$ to happen. Generally, to obtain the σ's, one has to apply the conservation of charge principle. This is done by solving the *Master Equation*:

$$\begin{aligned}\dot{\sigma}(\{n\}) = \sum_{j=1}^{N} \Big\{ & \sigma\,(\cdots, n_j - 1, n_{j+1} + 1, \cdots)\Gamma_j^-(\cdots, n_j - 1, n_{j+1} + 1, \cdots) \\ & + \sigma(\cdots, n_j + 1, n_{j+1} - 1, \cdots)\Gamma_j^+(\cdots, n_j + 1, n_{j+1} - 1, \cdots) \\ & - \left[\Gamma_j^+(\cdots, n_j, n_{j+1}, \cdots) + \Gamma_j^-(\cdots, n_j, n_{j+1}, \cdots)\right] \sigma(\cdots, n_j, n_{j+1}, \cdots)\Big\}.\end{aligned} \tag{7}$$

In the stationary state $\dot{\sigma}(\{n\}) = 0$, thus allowing one to solve for $\sigma(\{n\})$'s iteratively. In practice, however, obtaining the configuration probabilities is a tedious (even impossible) task, and one has to surpass this stage by, *e.g.*, using the symmetry properties of σ's in the specific problem under investigation, or by restoring to the Monte–Carlo simulations. The latter is the case for larger arrays, particularly.

Charging effects are strongly influenced by the electric circuit loading the junction. The circuit consists of a voltage (or current) source, and the *electromagnetic environment*. In a tunnel junction, as a consequence of the tunneling through the barrier, the voltage across the junction fluctuates. The electromagnetic environment, instead, is the source of dissipation in the circuit. Interestingly, however, dissipation and fluctuation in electric systems have mutual dependence on each other (cf. the *fluctuation–dissipation theorem*). The effect of electromagnetic environment is most pronounced for single tunnel junctions and, indeed, it has been pondered that without the environment, Coulomb blockade would be completely

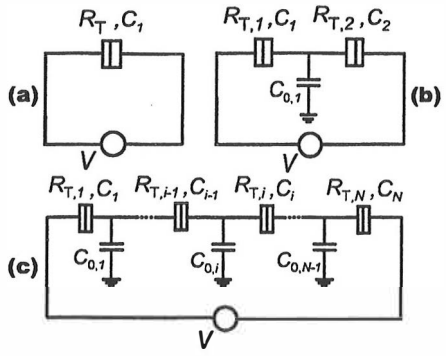

FIG. 1: (**a**) A single tunnel junction coupled to a perfectly biased voltage source, (**b**) a two–junction array, and (**c**) an array of N tunnel junctions.

suppressed in these systems [3]. Instead, charging effects are observable in arrays of tunnel junction even if the external impedance is vanishingly small. This is due to the charge quantization on the metallic islands between the junctions.

In practice, the (external) electromagnetic environment is modeled by an impedance, $Z_e(\omega)$, connected in series to the tunnel junction (Fig. 2). Here, once again, one is interested in obtaining the tunneling rates, Γ. Now, however, this is a more elaborate task. First of all, one should search for the proper quantum mechanical Hamiltonian of the electromagnetic environment, $H_{\rm env}$. We are not going to the details of such a Hamiltonian, and suffice to mention that, it is composed of *harmonic oscillators* (*i.e.* LC–elements), and, while deriving it, one uses the concepts of the *effective charge* on the junction,

$$\tilde{Q} \equiv Q - CV, \tag{8}$$

and the *effective phase* difference across it,

$$\tilde{\varphi}(t) \equiv \varphi(t) - \frac{e}{\hbar} V t. \tag{9}$$

Here the quantum–mechanically conjugate variables $\varphi(t) \equiv \frac{e}{\hbar}\int_0^t \mathrm{d}t' U(t')$ and $U(t) \equiv Q(t)/C$ are the phase and the voltage differences across the junction, respectively.

It has already been shown that any electromagnetic impedance can be modeled by an infinite number of harmonic oscillators $L_n C_n$. The corresponding Hamiltonian is, then, given

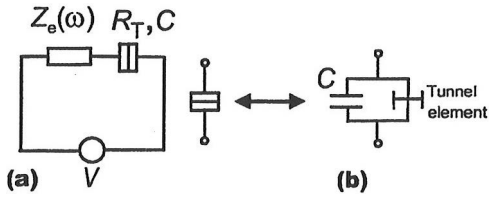

FIG. 2: **(a)** A single tunnel junction in electromagnetic environment $Z_e(\omega)$ coupled to a perfectly biased voltage source, **(b)** the tunnel element model for a tunnel junction used in the phase–correlation theory.

by [4]:

$$H_{\rm env} = \frac{\tilde{Q}^2}{2C} + \sum_{n=1}^{N} \left[\frac{q_n^2}{2C_n} + \left(\frac{\hbar}{e}\right)^2 \frac{1}{2L_n} (\tilde{\varphi} - \varphi_n)^2 \right], \tag{10}$$

with $\tilde{Q}$ and $\tilde{\varphi}$ defined in Eqs. (8)–(9). Here, q_n and φ_n are the charge on the n-th capacitor and the phase difference across it. In Eq. (10), the first term corresponds to the (effective) charging energy of the tunnel junction. The second term, instead, arises from the coupling of the environmental degrees of freedom to the (effective) phase difference across the junction. Such environmental degrees of freedom are represented by harmonic oscillators of frequencies $\omega_n \equiv 1/\sqrt{L_n C_n}$.

Furthermore, to describe the composed system of the environment and the tunnel junction itself, in addition to the Hamiltonian presented above, one should take the contribution of the electrons *and* the tunneling event into account. Assuming that the electrons on the electrodes of the junction constitute a system of non-interacting particles (which, due to the large density of such electrons and thereby screening effects, is justified), the electronic contribution to the total Hamiltonian can be expressed in terms of quasiparticle (number) operators, $c^\dagger c$, and the energy of such particles, ϵ, that is:

$$H_{\rm qp} \equiv \sum_{\ell\sigma} \epsilon_\ell c^\dagger_{\ell\sigma} c_{\ell\sigma} + \sum_{r\sigma} \epsilon_r c^\dagger_{r\sigma} c_{r\sigma}. \tag{11}$$

Here, indices ℓ and r denote the wave vectors of the quasiparticles on the left and right electrodes respectively, and σ stands for their spin quantum numbers.

The tunneling event itself is modeled by the Hamiltonian

$$H_{\rm T} \equiv \sum_{\ell r\sigma} T_{\ell r} c^\dagger_{r\sigma} c_{\ell\sigma} e^{-i\varphi} + \text{H.c.} \tag{12}$$

Here, $T_{\ell r}$ is the matrix element (transition probability amplitude) for the tunneling of an electron from the left electrode and in the state ℓ into the state r in the right electrode, and H.c. is the abbreviation for the Hermitian conjugate. The annihilation and creation of an electron on left and right sides of the tunnel barrier are represented by the operators $c_{\ell\sigma}$ and $c^{\dagger}_{r\sigma}$, respectively. The exponential factor, $e^{-i\varphi}$, determines the change of the junction charge, Q, by the charge of an electron, e, as a consequence of a tunneling event. This can easily be verified by utilizing the commutation relation $[\varphi, Q] = ie$, and noticing that $e^{i\varphi}Qe^{-i\varphi} = Q - e$. Indeed, the non-linearity of the current–voltage characteristic in a tunnel junction has its roots in this exponential factor, for it is the *only* operator in the Hamiltonian which accounts for the change of the capacitor charge. From a microscopic point of view, this factor can be interpreted as a correction to the probability amplitude, $T_{\ell r}$, in the tunneling Hamiltonian above [7]. The Hermitian conjugate term describes the same process in the reverse direction, *i.e.*, the tunneling of an electron from the right electrode to the left one.

As was the case with the definition of the effective phase difference across the junction, here too, one would like to relate the fluctuations of the system around equilibrium state to the Hamiltonians of the system more explicitly. In other words, we prefer to express the Hamiltonians above in terms of the effective parameters. At the same time, the physical description of the system should not be changed as a consequence of the new representation: the new *effective* Hamiltonians, $\tilde{H}_{\rm T}$ and $\tilde{H}_{\rm qp}$, should have the same eigenvalues and eigenfunctions as the original ones, $H_{\rm T}$ and $H_{\rm qp}$. This aim is achieved by introducing the unitary transformations [6]

$$\tilde{H}_{\rm T} \equiv U^{\dagger} H_{\rm T} U = \sum_{\ell r \sigma} T_{\ell r} c^{\dagger}_{r\sigma} c_{\ell\sigma} e^{-i\tilde{\varphi}} + \text{H.c.} \tag{13}$$

and

$$\begin{aligned} \tilde{H}_{\rm qp} &\equiv U^{\dagger} H_{\rm qp} U - i\hbar U^{\dagger} \frac{\partial}{\partial t} U \\ &= \sum_{\ell\sigma} (\epsilon_{\ell} + eV) c^{\dagger}_{\ell\sigma} c_{\ell\sigma} + \sum_{r\sigma} \epsilon_r c^{\dagger}_{r\sigma} c_{r\sigma}. \end{aligned} \tag{14}$$

Above, $U \equiv U(t)$ is the time–dependent unitary operator given by:

$$U(t) \equiv \prod_{\ell\sigma} \exp\left[i \frac{e}{\hbar} V t c^{\dagger}_{\ell\sigma} c_{\ell\sigma} \right]. \tag{15}$$

To calculate the tunneling rates, the tunneling Hamiltonian will be treated as a small perturbation, and the Fermi's golden rule will be utilized. This method turns out to be sufficient if the tunnel resistance, R_{T}, is larger than the quantum resistance, $R_{\mathrm{K}} \equiv h/e^2$. It is also assumed that before the tunneling process the system is in equilibrium state and, after tunneling, the equilibrium is reached again before the next tunneling event happens. This means that the time between two tunneling events should be larger than the relaxation time of the system. In fact, the condition $R_{\mathrm{T}} \gg R_{\mathrm{K}}$ could be interpreted to have its origin in the assumption of equilibrium state. The transition rate between the initial state, $\mid i\rangle$, and the final state, $\mid f\rangle$, is then

$$\Gamma_{i\to f} = \frac{2\pi}{\hbar} \mid \langle f \mid \tilde{H}_{\mathrm{T}} \mid i\rangle \mid^2 \delta(E_i - E_f). \tag{16}$$

Expressing the initial and the final states ($\mid i\rangle$ and $\mid f\rangle$, respectively) in terms of the quasiparticle state energy, $\mid E\rangle$, and the reservoir state energy, $\mid R\rangle$, as $\mid i\rangle \equiv \mid E_i\rangle\mid R_i\rangle$ and $\mid f\rangle \equiv \mid E_f\rangle\mid R_f\rangle$, the matrix elements in Eq. (16) become

$$\langle f \mid \tilde{H}_{\mathrm{T}} \mid i\rangle = \langle E_f \mid H_{\mathrm{T}}^{\mathrm{q}}\mid E_i\rangle\langle R_f \mid e^{-i\tilde{\varphi}}\mid R_i\rangle + \langle E_f \mid H_{\mathrm{T}}^{\mathrm{q}\dagger}\mid E_i\rangle\langle R_f \mid e^{+i\tilde{\varphi}}\mid R_i\rangle. \tag{17}$$

Here, $H_{\mathrm{T}}^{\mathrm{q}} \equiv \sum_{\ell r\sigma} T_{\ell r} c_{r\sigma}^{\dagger} c_{\ell\sigma}$ is the part of the tunneling Hamiltonian that acts in the quasiparticle space. The exchange of energy between the tunneling electron and its electromagnetic environment, in turn, is taken care by introducing the reservoir states. Notice that, in Eq. (17), each of the operators $H_{\mathrm{T}}^{\mathrm{q}}$ and $e^{-i\tilde{\varphi}}$ acts *solely* on the quasiparticle and the reservoir states, respectively.

Proceeding in much the same way as described in [6], one gets for the tunneling rates

$$\Gamma^{\pm}(V) = \frac{1}{e^2 R_{\mathrm{T}}} \int_{-\infty}^{+\infty} \mathrm{d}E \frac{E}{1 - \mathrm{e}^{-\beta E}} P(\pm eV - E), \tag{18}$$

where $P(E)$ is the *probability density function*, *i.e.* the probability that the tunneling electron exchanges energy E with the environment

$$P(E) \equiv \frac{1}{2\pi\hbar} \int_{-\infty}^{+\infty} \mathrm{d}t \exp\left[J(t) + i\frac{E}{\hbar}t\right] \tag{19}$$

and $J(t) \equiv \langle[\tilde{\varphi}(t) - \tilde{\varphi}(0)]\tilde{\varphi}(0)\rangle$ is called the *phase–phase correlation function*

$$J(t) = 2\int_{-\infty}^{\infty} \frac{\mathrm{d}\omega\, \mathrm{Re}[Z_{\mathrm{t}}(\omega)]}{\omega} \frac{\mathrm{e}^{-i\omega t} - 1}{R_{\mathrm{K}} \quad 1 - \mathrm{e}^{-\beta\hbar\omega}}. \tag{20}$$

Above, $Z_{\mathrm{t}}(\omega)$ is the *total* electromagnetic impedance as seen from the junction [6]. Notice that this is *not* the same as the *external* electromagnetic environment, $Z_{\mathrm{e}}(\omega)$, but includes it.

In practice, except in few special cases, the above integrals should be evaluated numerically. However, it is rather useful to know some general features of them. From Eq. (18), as one may intuitively expect, $\Gamma^{+}(V) = \Gamma^{-}(-V)$. Using the symmetry properties of the phase correlators, $\langle \mathrm{e}^{i\tilde{\varphi}(t)}\mathrm{e}^{-i\tilde{\varphi}(0)}\rangle$, it can be shown that $P(-E) = \exp(-\beta E)P(E)$ [6]. This relation is called *detailed balance symmetry*, and it implies that the probability for tunneling electron to *lose* energy to the environment (this will cause the excitement of the environmental modes) is smaller than the probability (but not zero) to *absorb* energy from the environment by the Boltzmann factor, $\exp(-\beta E)$, and this probability becomes negligible at lower temperatures. From this, one obtains the less trivial relation for the tunneling rates: $\Gamma^{-}(V) = \exp(-\beta eV)\Gamma^{+}(V)$. Moreover, the fact that $\int_{-\infty}^{+\infty} \mathrm{d}E P(E) = \exp[J(0)] = 1$, justifies the interpretation of $P(E)$ as the probability density function, and the the relation $\int_{-\infty}^{+\infty} \mathrm{d}E E P(E) = i\hbar J'(0)$ can be effectively used in the numerical calculations.

As the impedance of the environment becomes smaller, the $P(E)$ function approaches the delta function $\delta(E)$, and the Γ's in Eq. (18) become reminiscent of those introduced in Eq. (2). In the opposite limit, *i.e.* for a high–impedance environment, the integral in $P(E)$ function becomes Gaussian and one gets [6]:

$$P(E) = \frac{1}{\sqrt{4\pi E_{\mathrm{C}} k_{\mathrm{B}} T}} \exp\left[-\frac{(E - E_{\mathrm{C}})^2}{4E_{\mathrm{C}} k_{\mathrm{B}} T}\right]. \tag{21}$$

For very low temperatures, $k_{\mathrm{B}}T \ll E_{\mathrm{C}}$, the above expression reduces to the simpler one

$$P(E) = \delta(E - E_{\mathrm{C}}), \tag{22}$$

which means that in this limit the tunneling electron transfers *all* the energy involved in the tunneling event, *i.e.* the charging energy, to the environment. (Cf. the case in which the environmental impedance is zero and $P(E) = \delta E$.

Substituting for $P(E) = \delta(E - E_C)$ in the tunneling rate expression, Eq. (18), and evaluating the integral at $T = 0$, one gets

$$\Gamma^{\pm}(V) = \frac{1}{\pi\hbar}\frac{R_K}{R_T}(\pm eV - E_C)\Theta(\pm eV - E_C), \tag{23}$$

where $\Theta(x)$ is the unit step function [16]. The total current through the junction can then be obtained from the generally valid relation

$$I(V) = q\left[\Gamma^{+}(V) - \Gamma^{-}(V)\right] \tag{24}$$

by putting $q = e$ for the normal case, and using Eq. (23) above. The result reads:

$$I(V) = \frac{1}{eR_T}(eV - E_C)\Theta(eV - E_C). \tag{25}$$

Equation (25) is a formal verification for the Coulomb blockade effect at $T \simeq 0$. This result is in agreement with the very basic condition for "observing" Coulomb blockade presented in the previous section [Eq. (1)]: supposing that the voltage across the junction is V, current flows if $eV > E_C$.

Single Electron Transistor and Tunnel Junction Arrays

The techniques used to obtain the above results for a single tunnel junctions can be extended to derive the corresponding expressions for single electron transistor (SET) and larger one– and two–dimensional arrays. The only restriction is to neglect the higher order tunneling events (which, in practice, is well justified for most of the situations). For the case of sequential tunneling in an array with $N \geq 2$, while considering the junction in which the tunneling event happens, the rest of the array can be supposed as an electromagnetic environment to this junction in form of capacitors, and the similar formulae for tunneling rates *etc.* can be obtained. Here, as one can imagine, the charging energy of a junction in the array is not that convenient to evaluate, because it depends on the charge configuration on the islands and on the charge of the other junctions, as well as on the charge of stray capacitors. Besides this, the voltage difference across different junctions is not the same and one should be aware of this fact. It appears that the most effective way to present generally

valid expressions for the tunneling rates is to express them in terms of charge configuration on the islands, $\{n\} = \{n_1, n_2, \ldots, n_{N-1}\}$, and the change in the free energy of the *array*, δF_k, when electron tunnels through the k-th junction. Thus, for the tunneling rates through the k-th junction, one gets

$$\Gamma_k^{\pm}(\{n\}) \equiv \Gamma\left(\delta F_k^{\pm}(\{n\})\right) = \frac{1}{e^2 R_{\mathrm{T},k}} \int_{-\infty}^{+\infty} \mathrm{d}E \frac{E}{1 - \mathrm{e}^{-\beta E}} P_k(-\delta F_k^{\pm} - E). \tag{26}$$

Here $P_k(E) \equiv \frac{1}{(2\pi\hbar)} \int_{-\infty}^{+\infty} \mathrm{d}t \mathrm{e}^{[J_k(t) + i\frac{E}{\hbar}t]}$ is the corresponding probability density distribution and $J_k(t)$ accounts for the phase–phase correlation function of the junction k:

$$J_k(t) = 2 \int_{-\infty}^{\infty} \frac{\mathrm{d}\omega}{\omega} \frac{\mathrm{Re}[Z_t^k(\omega)]}{R_{\mathrm{K}}} \frac{\mathrm{e}^{-i\omega t} - 1}{1 - \mathrm{e}^{-\beta\hbar\omega}}, \tag{27}$$

where $Z_t^k(\omega)$ is the *total* impedance of the circuit *as seen from the k-th junction.*

One more useful relation for the tunneling rates can be derived by imposing the expression of $P_k(E)$ into Eq. (26), and by applying the Fourier transform techniques:

$$\Gamma_k^{\pm}(\{n\}) = \frac{1}{e^2 R_{\mathrm{T},k}} \left\{ \frac{1}{\beta} + \frac{-\delta F_k^{\pm} - i\hbar J_k'(0)}{2} - \frac{\pi}{2\beta^2\hbar} \mathcal{P} \int_{-\infty}^{+\infty} \mathrm{d}t \frac{\mathrm{e}^{[J_k(t) - i\delta F_k^{\pm}\frac{t}{\hbar}]} - 1}{\sinh^2(\frac{\pi t}{\beta\hbar})} \right\}. \tag{28}$$

Above, $\mathcal{P}$ stands for the principal value of the integral. In practice, this integral (as well as those formerly appeared) can be numerically evaluated by decomposition of it to the real and imaginary parts and by using the symmetry properties of the expressions thus obtained. This way, one avoids integrating over improper values, and speeds up the calculation procedure. In principle the number of charge configurations on the islands is infinite, and one does not know the initial distribution of them. After each tunneling event, the configuration changes and the integrals above should be re-evaluated. This means that for larger arrays the numerical simulation of the charge transfer through the junctions becomes a very time–consuming procedure. To overcome this bottleneck, one should resort to the Monte–Carlo simulations. The basic idea here is to study a finite number of "randomly" chosen states of the system and to derive the underlying physics out of these. In what follows, I will have an overview on this method, and present the algorithms involved in this work.

2.2 The Monte–Carlo Simulations

The algorithm used here has already been described in more detail in [8] and is a slightly modified version [9] of that developed in [10].

Let us suppose that the array is initially in the state $\{n\}$. The probability that this state changes as the consequence of a tunneling event in junction k, is equal to

$$f_k^{\pm} \equiv f_k^{\pm}(\{n\}) = \frac{\Gamma_k^{\pm}(\{n\})}{\sum_{k=1}^{N}[\Gamma_k^{+}(\{n\}) + \Gamma_k^{-}(\{n\})]}. \tag{29}$$

The *expected* "lifetime" of the state $\{n\}$, *i.e.* the time the array spends on average in this configuration, is

$$\delta t(\{n\}) \equiv \left\{\sum_{k=1}^{N}\left[\Gamma_k^{+}(\{n\}) + \Gamma_k^{-}(\{n\})\right]\right\}^{-1}. \tag{30}$$

At different moments of time, the system can be arbitrarily many times in any state $\{n\}$. Let us mark the number associated with $\{n\}$ by $S_{\{n\}}$. Then, the (expected) total time spent in $\{n\}$, *the associated time*, is

$$\Delta t(\{n\}) \equiv S_{\{n\}}\delta t(\{n\}), \tag{31}$$

and the net amount of charge transferred through the k-th junction during this time interval will be

$$qS_{\{n\}}(f^{+} - f^{-}). \tag{32}$$

The total current through the k-th junction, I_k, can then be obtained by dividing the net charge transformed through the junction [by summing the partial charges transformed in Eq. (32) over all the states $\{n\}$], by the total time needed for this process [by summing Eq. (31) over the corresponding states]:

$$I_k = q\frac{\sum_{\{n\}}\left\{S_{\{n\}}\frac{\Gamma_k^{+}(\{n\})-\Gamma_k^{-}(\{n\})}{\sum_{k=1}^{N}[\Gamma_k^{+}(\{n\})+\Gamma_k^{-}(\{n\})]}\right\}}{\sum_{\{n\}}\{\Delta t(\{n\})\}}. \tag{33}$$

In the stationary state, the current through each junction should be the same, $I \equiv I_1 = I_2 = \cdots = I_N$. Assigning a weight w_k to each current I_k, and putting $\sum_{k=1}^{N} w_k = 1$, for the

stationary state, one obtains[†]

$$I = \sum_{k=1}^{N} I_k w_k = I \sum_{k=1}^{N} w_k. \tag{34}$$

The expression for current $I = I_k$, then, becomes:

$$I = \frac{q \sum_{\{n\}} \left\{ S_{\{n\}} \sum_{k=1}^{N} \left(\frac{\Gamma_k^+(\{n\}) - \Gamma_k^-(\{n\})}{\sum_{i=1}^{N} [\Gamma_i^+(\{n\}) + \Gamma_i^-(\{n\})]} \right) w_k \right\}}{\sum_{\{n\}} \{\Delta t(\{n\})\}}. \tag{35}$$

Here, the numerator can be interpreted as the total charge passed through the array $\Delta Q \equiv \sum_{\{n\}} \Delta Q(\{n\})$, and the denominator as the total time needed for this process $\Delta t \equiv \sum_{\{n\}} \Delta t(\{n\})$. In practice, the summations cannot be implemented over all the configurations $\{n\}$, and one should resort to a limited set of them, *i.e.* to those randomly *visited*, $\{n\}_v$, while taking the underlying physics of the problem into account. The current through the array can then be written as:

$$I = \frac{\Delta Q}{\Delta t} = \frac{\sum_{\{n\}_v} \Delta Q(\{n\}_v)}{\sum_{\{n\}_v} \Delta t(\{n\}_v)}, \tag{36}$$

or equivalently

$$I = \sum_{\{n\}_v} \left\{ q \frac{\sum_{k=1}^{N} [\Gamma_k^+(\{n\}) - \Gamma_k^-(\{n\})] w_k}{\sum_{k=1}^{N} [\Gamma_k^+(\{n\}) + \Gamma_k^-(\{n\})]} \right\} \frac{1}{\sum\limits_{\{n\}_v} \left(\sum_{k=1}^{N} [\Gamma_k^+(\{n\}) + \Gamma_k^-(\{n\})] \right)^{-1}}. \tag{37}$$

Notice that the number of visits $S_{\{n\}}$ no longer appears in Eq. (37), since it is already taken into account by performing the summation over all visited states *explicitly*. The simulation process starts from an arbitrary initial state, *e.g.* $\{n\}_0 \equiv \{0, 0, \ldots, 0\}$. The next state is obtained by dividing the interval $[0, 1]$ into segments whose lengths are proportional to the tunneling rates for this configuration and by *drawing* a random number, r, in this interval. The segment which r corresponds to specifies the junction through which the tunneling event happens and the direction ($\pm$) of this tunneling. Next, re-arranging the charge configuration

[†] If the array is not in stationary state the currents I_k are no more necessarily equal, and one should assign a weight to each of them. A reasonable choice for weights would be $w_k = R_{\mathrm{T},k}/R_\Sigma$, where $R_\Sigma \equiv \sum_{k=1}^{N} R_{\mathrm{T},k}$. This is so because one may expect that the current through each junction is proportional to the voltage difference across it. The voltage drop across junction k with resistance $R_{\mathrm{T},k}$, in turn, is expected to be proportional to $R_{\mathrm{T},k}/R_\Sigma$.

on the islands, $\{n\}_0 \rightarrow \{n\}_1$, the new tunneling rates for this configuration can be calculated. This process will be continued until a "sufficient" number of the states and the corresponding tunneling rates are obtained. [In practice, at $T = 4.2$ K, the results obtained by a rather small number of draws, ~ 10, agree within better that 1.5% accuracy (with respect to the depth and the half–width of the conductance curve around zero bias voltage) with those obtained from "long simulations" with number of draws in the range ~ 1000.] Tabulating these values, one can evaluate the summations in Eq. (37) and derive the current. Notice that the number of visits $S_{\{n\}}$ shown in Eq. (35) no longer appears here; it is taken into consideration in the simulation process itself.

The advantage of the algorithm explained is that it is not restricted to any specific theory, and can be equally utilized by different approaches.

2.3 The Strong Tunneling Regime

If $R_T \gg R_K$, the tunneling Hamiltonian can be treated as a perturbation and the golden rule can be utilized. On the other hand, as the junction resistance R_T becomes smaller, the tunneling frequency increases (R_T is inversely proportional to the square of the tunneling matrix element [6]) and there remains shorter and shorter time for the system to recover to a stable quantum mechanical state. Eventually, in the so-called *strong tunneling* (ST) regime, $R_T \ll R_K$, the initial and the final states of the system in a tunneling process are not well defined and one cannot use the perturbative approach previously described —at least in its original form.

To study the ST, we have used three different approaches: **1)** the modified phase–correlation (perturbative) theory, **2)** the path–integral technique, and **3)** the quasiclassical Langevin equation model.

2.3.1 The Extended Phase–correlation Theory

In a fairly recent model put forward by Joyez *et al.* [11], the authors propose that a high–conductance tunnel junction with $G_T \gg G_K$ [$G_K \equiv e^2/h$ is the quantum conductance],

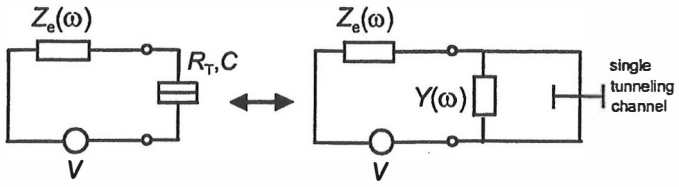

FIG. 3: Tunneling channel model for a single tunnel junction in an electromagnetic environment. $Y(\omega)$ is the admittance of the junction, and in addition to the capacitive part, it includes the contribution of the tunnel element itself —excluding the channel in which tunneling happens.

can be supposed as to be composed of a large number of *channels*, $G_T = \sum_k g_k$, each of which has a conductance g_k in the weak tunneling regime, $g_k \ll G_K$. Since electrons tunnel one at a time, one can assume that at the moment of tunneling only one channel is open, and the rest of them act as an implicit "electromagnetic environment" to the junction. Because all the channels experience the same voltage difference across the tunnel junction, one may expect that the (equivalent) environmental impedance of them should be coupled in parallel with the tunnel element itself (Fig. 3). In fact, this is very reminiscent of what we have already assumed for a junction in the weak tunneling regime. Here, the only difference is that, while evaluating the total environmental impedance $Z_t(\omega)$, one should account for the environment as it is seen from the *channel* in which the tunneling happens.

Supposing that the number of channels in a typical tunnel junction N_{ch} is large enough[†], the environmental contribution of the remaining $N_{ch} - 1$ channels to the one in which tunneling happens can be well approximated (within the order of $1/N_{ch}$) to be equal to the *whole* admittance (or impedance) of the junction itself. So, one should seek for a generally valid expression for the frequency-dependent complex admittance, $Y(\omega)$ of the junction.

[†] A rough estimate of the number of channels N_{ch} in a typical tunnel junction with an area of about 0.01 μm^2 can be obtained as follows: Since the tunneling electrons are those in the vicinity of the Fermi surface, they have wavelengths of the order of Fermi wavelengths, *i.e.*, few nanometers (for aluminum $\lambda_F \simeq$ 3.6 nm), that is, one can suppose that a tunneling electron "occupies" an area of about 10 nm^2, which in turn means that in a typical junction there should be "space" for about one thousand tunneling electrons, $N_{ch} \sim 1000$.

Fortunately, such a calculation has already been done and the result is [12]:

$$Y(\omega) = G_{\mathrm{T}} \left\{ 1 + \frac{2}{\pi} \mathcal{P} \int_0^\infty \mathrm{d}t \left[\frac{\pi/\hbar\beta}{\sinh(\pi t/\hbar\beta)} \right]^2 \mathrm{Im}\left[\mathrm{e}^{J(t)} \right] \frac{\mathrm{e}^{-i\omega t} - 1}{-i\omega} \cos\left(\frac{eVt}{\hbar} \right) \right\}. \qquad (38)$$

Above, $\mathcal{P}$ stands for the principal value of the integral and $J(t)$ is the familiar phase–phase correlation function introduced in Eq. (20). Note that here $Z_{\mathrm{t}}(\omega) \equiv Z_{\mathrm{e}}(\omega) \mid\mid Y^{-1}(\omega)$ is the total impedance of the junction as seen from the *channel element* in this junction (Fig. 3). Since the complex admittance $Y(\omega)$ appears in both the expressions (20) and (38), one should solve for it self–consistently. A good choice for initial value of admittance is to put $Y(\omega) = G_{\mathrm{T}}$. In practice, $Y(\omega)$ can be evaluated within few iterations. The results of such a calculation at zero bias voltage for different temperatures and for different junction parameters are given in [11]. It appears that at not very high temperatures $Y(\omega)$ has a strong frequency dependence. In fact, evaluating the complex admittance of a tunnel junction may have more general applications in the future, if working with high frequencies ($\sim$ 1 GHz) becomes a routine in the single electron experiments. Finally, it should be pointed out that the only hypothesis in deriving Eq. (38) is that the (external) electromagnetic environment should be in thermal equilibrium with its surroundings [11, 12]. This, in turn, means that the current through the junction has to be not very large, otherwise dissipation heats the environment [11]. The extension of the channel model to arrays of tunnel junctions is straightforward: In Eq. (38), $Y(\omega)$, G_{T}, and $J(t)$ should be replaced by their equivalents for the k-th junction in an array, *i.e.* by $Y_k(\omega)$, $G_{\mathrm{T},k}$, and $J_k(t)$, respectively.

2.3.2 The Path–integral Method

In this method, introducing the concept of imaginary time, $\tau \equiv it$, one can present the quantum mechanical time evolution operator of a system with Hamiltonian $\hat{H}$, $\hat{U}(t) \equiv \exp(-it\hat{H}/\hbar)$, in a form familiar from thermodynamics, $\hat{U}(\tau) = \exp(-\tau\hat{H}/\hbar)$. The thermodynamic partition function of a system, $\mathcal{Z} \equiv Tr \exp(-\beta\hat{H})$, can be written in terms of (classical) phase–space parameters, *i.e*, in terms of the position x and the linear momentum

$\dot{x}$ as a path–integral[†]

$$\mathcal{Z} = \int\limits_{x(0)=x(\beta\hbar)} \exp\left\{-\frac{1}{\hbar}S[x(\tau),\dot{x}(\tau)]\right\}\mathcal{M}[x(\tau)], \tag{39}$$

where

$$S[x(\tau),\dot{x}(\tau)] = \int\limits_0^{\beta\hbar} H(\tau)\mathrm{d}\tau \tag{40}$$

is the *Euclidian action* (like in Lagrangian mechanics) and $\mathcal{M}[x(\tau)]$ is the *measure* of integration.

Let us apply the above technique to the case of a single tunnel junction and its electromagnetic environment. The conjugate variables now are the phase difference across the junction and the charge on it (or, equivalently, the charging energy of the junction), so that one would expect to see these parameters in the Euclidian action describing the system. In fact, this is the case and the partition function can be written as

$$\mathcal{Z}[\xi] = \int \exp\left\{-\frac{1}{\hbar}S[\varphi,\xi]\right\}\mathcal{M}[\varphi]. \tag{41}$$

Above, φ is the phase and $\xi \equiv \xi(\tau)$ is the related variation parameter [14]. The action S now can be decomposed to three different parts: $S[\varphi,\xi] \equiv S_{\mathrm{C}}[\varphi] + S_{\mathrm{T}}[\varphi] + S_{\mathrm{e}}[\varphi,\xi]$, where

$$S_{\mathrm{C}}[\varphi] \equiv \int\limits_0^{\beta\hbar} \frac{\hbar^2}{4E_{\mathrm{C}}}\dot{\varphi}^2\mathrm{d}\tau \tag{42}$$

is the contribution of the charging energy E_{C} to the action and

$$S_{\mathrm{T}}[\varphi] \equiv 2\int\limits_0^{\beta\hbar}\int\limits_0^{\beta\hbar} \alpha(\tau-\tau')\sin^2\left[\frac{\varphi(\tau)-\varphi(\tau')}{2}\right]\mathrm{d}\tau'\mathrm{d}\tau \tag{43}$$

describes the tunneling of quasiparticles through the junction. The kernel $\alpha(\tau)$ depends on the ratio of the quantum and the junction resistances, and can be written in terms of Matsubara frequencies $\omega_n \equiv 2\pi n/\hbar\beta$ as:

$$\alpha(\tau) \equiv \frac{1}{\hbar\beta}\sum_{n=-\infty}^{\infty}\tilde{\alpha}(\omega_n)e^{-i\omega_n\tau}; \qquad \tilde{\alpha}(\omega_n) \equiv -\frac{\hbar}{4\pi}\frac{R_{\mathrm{K}}}{R_{\mathrm{T}}}\mid\omega_n\mid. \tag{44}$$

[†] It is worth–noticing that the idea of path–integral has its roots in the classical ***Lagrangian*** mechanics (the ***Hamiltonian*** representation). Here, once again, one uses the conjugate variables x and $\dot{x}$, but now named as the phase–space parameters [13].

The contribution of the electromagnetic environment to the action takes the form

$$S_e[\varphi,\xi] \equiv \frac{1}{2}\int_0^{\beta\hbar}\int_0^{\beta\hbar} \kappa(\tau-\tau')\left[\varphi(\tau)+\frac{e}{\hbar}\xi(\tau)-\varphi(\tau')-\frac{e}{\hbar}\xi(\tau')\right]\mathrm{d}\tau'\mathrm{d}\tau. \tag{45}$$

Above, the kernel $\kappa(\tau)$ depends on the properties of the environment and it is given in [14]. Finally, for the differential conductance of the junction at zero bias voltage, $G(0)$, one derives [14]

$$G(0) \equiv \left.\frac{\mathrm{d}I}{\mathrm{d}V}\right|_{V=0} = \lim_{\omega\to 0}\frac{1}{\hbar\omega}\mathrm{Im}\left[\lim_{i\omega_n\to\omega+i\delta}\int_0^{\beta\hbar} e^{i\omega_n\tau}\langle I(\tau)I(0)\rangle\right]\mathrm{d}\tau. \tag{46}$$

Here, the current correlation function, $\langle I(\tau)I(0)\rangle$, can be expressed in terms of the partition function in Eq. (41) as:

$$\langle I(\tau)I(0)\rangle = \frac{\hbar^2}{\mathcal{Z}[0]}\left.\frac{\delta^2\mathcal{Z}[\xi(\tau)]}{\delta\xi(\tau)\delta\xi(0)}\right|_{\xi(\tau)=0}. \tag{47}$$

For the case of a purely resistive environment, the kernel appearing in Eq. (45) becomes

$$\kappa(\tau) \equiv \frac{1}{\hbar\beta}\sum_{n=-\infty}^{\infty}\tilde{\kappa}(\omega_n)e^{-i\omega_n\tau}; \qquad \tilde{\kappa}(\omega_n) \equiv -\frac{\hbar}{4\pi}\frac{R_K}{R_e}\mid\omega_n\mid. \tag{48}$$

The similarity between Eqs. (44) and (48) can be understood rather easily: the action S_e should depend on the environmental resistance R_e exactly in the same way as S_T depends on the tunnel resistance R_T.

In the high temperature limit $k_BT \gg E_C$, using a series expansion for $S_0[\varphi] \equiv S[\varphi,\xi=0]$ with βE_C as the expansion parameter, one finds [14, 15]

$$S_0[\varphi] = \int_0^{\beta\hbar}\frac{\hbar^2}{4E_C}\dot{\varphi}^2\mathrm{d}\tau + \frac{1}{2}\int_0^{\beta\hbar}\int_0^{\beta\hbar}\alpha_{tot}(\tau-\tau')\left[\varphi(\tau)-\varphi(\tau')\right]\mathrm{d}\tau'\mathrm{d}\tau, \tag{49}$$

where $\alpha_{tot}(\tau) \equiv \alpha(\tau)+\kappa(\tau)$. Inserting this expression into Eq. (41), and performing the limit in Eq. (46), one gets [14]:

$$\begin{aligned}\left(\frac{1}{G_T}+\frac{1}{G_e}\right)G_{tot}(0) &= 1-\frac{\beta E_C}{3}\frac{R_T}{R_T+R_e}\\ &+(\beta E_C)^2\left[\frac{1}{15}\frac{R_T}{R_T+R_e}+\frac{3\zeta(3)R_K}{4\pi^4R_e}\right]+\mathcal{O}\left[(\beta E_C)^3,\frac{R_e}{R_T}(\beta E_C)^2\right].\end{aligned} \tag{50}$$

Above, $\zeta(x)$ is the zeta function [16], and $G_{\rm tot}$ is the total, *i.e.*, the resultant conductance of the junction and the environment together. It is noticeable that when $R_{\rm T} \to \infty$ this result coincides with the expression of conductance obtained for the high temperature limit in the weak tunneling regime [5, 17]. Furthermore, assuming that $(R_{\rm K}/R_{\rm e})(\beta E_{\rm C})^2 \ll 1$, a linear dependence between the dip of the conductance curve at zero bias voltage, $\Delta G \equiv G_{\rm T} - G(0)$, and temperature T can be obtained [14]:

$$\left(\frac{\Delta G}{G_{\rm T}}\right)^{-1} = \frac{3k_{\rm B}T}{E_{\rm C}} + \delta, \tag{51}$$

where δ depends on the ratio of the quantum and environmental resistances, as well as on the ratio of the quantum and asymptotic junction resistances:

$$\delta \equiv \frac{3}{5} + \frac{27\zeta(3)}{2\pi^4}\left(\frac{R_{\rm K}}{R_{\rm e}} + \frac{R_{\rm K}}{R_{\rm T}}\right) + \frac{R_{\rm e}}{R_{\rm e}+R_{\rm T}}. \tag{52}$$

2.3.3 The Quasiclassical Langevin Equation Approach

In the most general form, the classical Langevin equation can be written as:

$$\alpha\frac{{\rm d}^2x}{{\rm d}t^2} + \beta\frac{{\rm d}x}{{\rm d}t} = y(t). \tag{53}$$

To get some insight to the physical meaning of different terms in Eq. (53), one may compare it to the familiar equation of motion of a particle in a dissipative medium under a constant potential. The first term represents the "inertia" of the particle, and the second one is the "friction" term. The righthand side, correspondingly, is the time-dependent "external force". The essential difference, however, between the classical dissipation equation and the so-called (classical) Langevin equation is that the "external force" in the latter one has stochastic, *i.e.* random, nature. For example, the thermal fluctuations of electrons in a resistor, which are the source of the so-called Johnson–Nyquist noise, have such a nature. Another example is the Brownian motion of extremely small particles in a liquid.

All the time, especially while considering quantum systems, one deals with different kinds of fluctuations: fluctuation of charge on a capacitor, thermal fluctuations of electrons in a metal, fluctuation of phase across a Josephson junction, and so on. In the majority

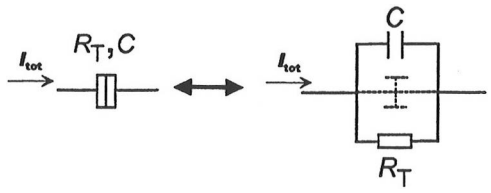

FIG. 4: A single tunnel junction together with its equivalent circuit model used in the quasiclassical Langevin equation approach. In the case of a superconducting tunnel junction, the supercurrent passes through the dashed element.

of cases, probably even in all of them, fluctuations in "small" systems have a quantum mechanical origin. Indeed, from a fundamental point of view, one may conjecture that fluctuations have their root in the discreteness of physical quantities. That is why the fluctuations become more important as the system becomes "smaller", and, in fact, in some cases their consideration is vital for a satisfactory description of the physical phenomena. As a representative example, one may mention the well known "white noise" (the Johnson–Nyquist noise). Another example is the shot noise —which is a consequence of discreteness of electric charge [19, 20].

Usually, the time-dependent "force" on the righthand side of Eq. (53) can be supposed as composed of two parts: the "principal" value and the noise, *i.e.* the (quantum) fluctuations, imposed on the principal value. Furthermore, in a real quantum system, the classical quantities on the left-hand side of the Langevin equation have to be substituted by their quantum mechanical counterparts. For instance, in the case of a single tunnel junction, one may apply the classical Ohm's law for conservation of charge, and using the correspondence between the classical and the (quantum) electrical quantities, write for the relevant quantum Langevin equation. To be more explicit, let us consider the situation depicted in Fig. 4. The total current, $I_{\rm tot}$, passing through the junction can be written as:

$$I_{\rm tot} \equiv I + I_{\rm n}(t). \tag{54}$$

Here, I and $I_{\rm n}(t)$ are the principal (bias) and the noise current, respectively. Using the

tunnel element model shown in the figure, and applying the Ohm's law, we obtain

$$C\frac{\hbar\ddot{\theta}}{e}+\frac{1}{R_{\mathrm{T}}}\frac{\hbar\dot{\theta}}{e}=I+I_{\mathrm{n}}(t). \tag{55}$$

Above, $\theta(t)\equiv\frac{e}{\hbar}\int_{-\infty}^{t}\mathrm{d}t'V(t')$ is the phase (difference) across the junction. (The definition of phase here differs from that of a Josephson junction just by a factor $2=2e/e$.) The first term in Eq. (55) is the current passing through the capacitor, and the second one is the dissipation current, *i.e.* the current which passes through the resistor. Similarly, for a superconducting tunnel junction, there should be one additional term on the left side of the equation, namely the Josephson supercurrent passing through the tunnel element (the dashed part in Fig. 4). In fact, originally, the quantum Langevin approach was developed for superconducting tunnel junctions [19].

The main objective now is to find the explicit form of the quantum noise current, $I_{\mathrm{n}}(t)$, above. This is not a simple task. Attempts to describe the noise in quantum systems go back to, at least, as early as 1951 [21]. Widely speaking, there have been two types of efforts. One of them has a more general nature, *i.e.* introducing the quantum noise for a wide range of systems in a rather general form [4, 21]. The other one, instead, was an attempt to find a phenomenological quantum equation, *i.e.* the "quantum Langevin equation", for the specific problem presented above [22, 23]. To get more insight to what will be introduced in the following lines, it would be useful to have a closer look at these approaches.

It was shown, already long time ago, that the current noise through a linear element with resistance R and with ideal Gaussian fluctuations, is (to a good extent) independent of the state of the system. The power spectrum of this current is given by [21]:

$$S_I(\omega)=\frac{1}{R}\hbar\omega\coth\left(\frac{\hbar\omega}{2k_{\mathrm{B}}T}\right). \tag{56}$$

However, by reducing the size of the system, the contribution of non–Gaussian fluctuations to the noise becomes more important, and one needs more details about the quantum noise. In such systems, the noise depends on the state of the system. As an example, let us mention the small-area tunnel junctions. Here, the elementary process is the *discrete* single electron tunneling, and the noise is shot noise.

In a small tunnel junction, assuming that the (classical) electrons are traversing the tunnel barrier, the current can be supposed to be the sum of independent events,

$$I(t) = e\sum_i \delta(t - t_i) - e\sum_j \delta(t - t_j), \tag{57}$$

where the distribution of times (t_i and t_j for forward and backward transitions, respectively) is Poissonian. For a voltage-biased junction, the mean current becomes $\langle I(t)\rangle = V/R$ and the fluctuations in the current, $I_{\rm n}(t) = I - \langle I\rangle$, depend on the bias voltage and the asymptotic tunnel resistance $R_{\rm T}$ as [20]:

$$\begin{aligned}\langle I_{\rm n}(t) I_{\rm n}(t')\rangle &= \frac{eV}{R_{\rm T}}\left[\mathcal{B}(eV) - \mathcal{B}(-eV)\right]\delta(t-t') \\ &= \frac{eV}{R_{\rm T}}\coth\left(\frac{eV}{2k_{\rm B}T}\right)\delta(t-t').\end{aligned} \tag{58}$$

Above, $\mathcal{B}(x) \equiv 1/(1 - {\rm e}^{-x})$ is the Bose function. For large voltages, $eV \gg k_{\rm B}T$, the fluctuations are proportional to the mean current itself. This is in accordance with the expected characteristic feature of shot noise.

The power spectrum of a (normal) tunnel junction can also be derived quantum–mechanically [24]. The result reads

$$S_I(\omega) = \frac{1}{2}\sum_{m=\pm 1}\frac{eV + m\hbar\omega}{R_{\rm T}}\coth\left(\frac{eV + m\hbar\omega}{2k_{\rm B}T}\right). \tag{59}$$

In the limit of small frequencies or higher voltages, $\hbar\omega \ll eV$, the above result reduces to that of Eq. (58). It is noticeable that contrary to the simpler result of Eq. (56), the noise here depends on the state of the system, *i.e.* on the voltage V. In reality, there is a mutual dependence between the state of the system and the shot noise, and the treatment of the problem is much more complicated. A thorough study of this problem can be found in Ref. [20]. However, the expressions appearing in the more detailed treatments of the noise look very much the same as the equations presented above; the underlying physics is essentially the same.

There have also been another type of efforts —mainly based on intuition and phenomenology— to describe the noise current in Eq. (55), and to introduce a "quantum Langevin equation" for a tunnel junction with resistance $R_{\rm T}$ [23]-[25]. In the simplest

case, the noise correlation function has been suggested to have a form reminiscent of that in Eq. (56), that is, $(\hbar\omega/R_{\rm T})\coth(\hbar\omega/2k_{\rm B}T)$. This expression follows from the modeling of the Johnson–Nyquist noise across a resistor. There have also been other attempts to generalize the simple expression introduced to the systems with temporary bias voltage $V(t)$. This way, *i.e.* by suggesting a noise correlation function of the form appearing in Eq. (58) with V substituted by its time-dependent counterpart $V(t)$, the authors in Ref. [25] have attempted to take the mutual influence between the noise and the state of the system into consideration. However, despite its suggestive form, this idea, too, is insufficient for a satisfactory description of the noise. The reason is that, in general, if $V(t)$ varies on a time scale comparable to or faster than $\hbar/k_{\rm B}T$, this model violates the fluctuation–dissipation theorem [19, 20].

After these preliminary remarks on the correct form of the noise current in the quantum Langevin equation, let us return to a consideration of our main goal and present the proper expression for the quantum noise and its correlation functions.

The exact, quantum–mechanically consistent, form of the shot noise $I_{\rm n}(t)$ in Eq. (55) can be obtained by introducing the "center-of-mass" $\theta \equiv \frac{1}{2}(\theta_1+\theta_2)$, and the "relative" $\chi \equiv \frac{1}{2}(\theta_1-\theta_2)$ (phase) coordinates, and by applying the least action principle:

$$\left.\frac{\delta S[\theta,\chi,\xi_i]}{\delta\chi}\right|_{\chi=0} = 0. \tag{60}$$

Above, S is the (complex) action and $\xi_i(t)$ with $i=1,2$ are independent Gaussian random variables with the correlation functions given in [19]. The current noise is thus given by

$$I_{\rm n}(t) = \xi_1(t)\cos[\theta(t)] + \xi_2(t)\sin[\theta(t)], \tag{61}$$

where for the correlations of ξ_i

$$\langle \xi_i \xi_j \rangle_\omega = \delta_{ij}\frac{\hbar\omega}{R_{\rm T}}\coth\left(\frac{\hbar\omega}{2k_{\rm B}T}\right). \tag{62}$$

The Langevin description presented above has its limitations and one should pay enough attention to its validity range. In the classical limit ($\hbar\omega, eV \ll k_{\rm B}T$) this description is precise enough [19, 20], and the expression for noise, Eq. (62), reduces to that of the classical

white Gaussian noise. Beyond the classical regime, the current noise is still given by Eqs. (61) and (62), provided that the voltage is constant or nearly constant, $V(t) - \langle V \rangle \ll \langle V \rangle$. [This is true even if $e\langle V \rangle \gtrsim k_B T \gg \hbar\omega$.] In general, from microscopic theory, it can be shown that the Langevin description is sufficient in the classical limit and in the limit of strong damping, $\hbar/e^2 R_T \gg 1$, that is, for high–conductance tunnel junctions [20].

More recently, Golubev† and Zaikin have extended the Langevin equation approach to the case of a single tunnel junction with an arbitrary external impedance $Z_e(\omega)$ connected in series with the junction (cf. Fig. 2). Their result reads [26]:

$$C\frac{\hbar\ddot{\varphi}}{2e} + \frac{1}{R_T}\frac{\hbar\dot{\varphi}}{2e} + \int \hat{Z}_e^{-1}(t-\tau)\frac{\hbar\dot{\varphi}(\tau)}{2e}d\tau - \frac{V_x}{Z_e(0)} = \frac{\xi_v(t)}{R_T}\sin\left(\frac{\varphi}{2}\right) + \frac{\xi_w(t)}{R_T}\cos\left(\frac{\varphi}{2}\right) + \xi_e(t), \tag{63}$$

where V_x stands for the external bias voltage and ξ_v, ξ_w, and ξ_e are Gaussian stochastic variables*

$$\langle \xi_v(t_1)\xi_v(t_2)\rangle = \langle \xi_w(t_1)\xi_w(t_2)\rangle = R_T\mathcal{G}(t_1 - t_2); \tag{64}$$
$$\langle \xi_e(t_1)\xi_e(t_2)\rangle = \int \frac{d\omega}{2\pi}\mathrm{Re}\left[\frac{\hbar\omega}{Z_e(\omega)}\right]\coth\left(\frac{\hbar\omega}{k_B T}\right)\exp[-i\omega(t_1 - t_2)].$$

with

$$\hat{Z}_e(t) \equiv \int \frac{d\omega}{2\pi} Z_e(\omega)\exp(-i\omega t), \tag{65}$$
$$\hat{Z}_e^{-1}(t) \equiv \int \frac{d\omega}{2\pi}\frac{1}{Z_e(\omega)}\exp(-i\omega t);$$

and

$$\mathcal{G}(t) \equiv \int \frac{d\omega}{2\pi}\hbar\omega\coth\left(\frac{\hbar\omega}{2k_B T}\right)\exp(-i\omega t) = -\frac{1}{\pi\hbar}\frac{(\pi k_B T)^2}{\sinh^2\left(\frac{\pi k_B T t}{\hbar}\right)}. \tag{66}$$

All the integrals above should be performed over the interval from $-\infty$ to $+\infty$.

---

† I am grateful to Dmitri S. Golubev for his clarifying comments on the subject.

* The correlation functions in Eq. (64), as well as those in Eqs. (56) and (61), have their roots in the **fluctuation–dissipation theorem**: the power spectrum of current fluctuations at frequency ω is proportional to the imaginary part of the conductance of the system at the same frequency multiplied by $\hbar\omega\coth(\hbar\omega/2k_B T)$. It is worth–noticing that replacing the phase θ in Eq. (61) by eVt, and using Eq. (62), one can find the average $\langle I_n(t)I_n(0)\rangle$. Equation (59) can be obtained by taking the Fourier transform of this average.

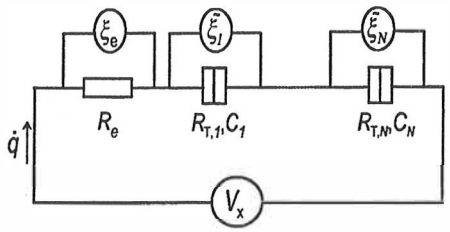

FIG. 5: A one-dimensional array of normal-metal tunnel junctions with resistive electromagnetic environment. For notation, see the text.

The first two terms on the righthand side of Eq. (63) stand for the shot noise of a tunnel junction [cf. Eq. (61)], while the last term is the Gaussian noise of the electromagnetic environment. The third and fourth term on the left-hand side of Eq. (63), together, are the average current through the circuit. Also, notice that the phase here is defined as it is commonly defined for the Cooper pairs, $\varphi(t) \equiv \frac{2e}{\hbar}\int_0^t \mathrm{d}t' V(t')$. This, however, is only a formal matter, since the effect of factor 2 in front of the electron charge, e, can easily be suppressed into definition of the correlation relations above. In the rest part of this thesis, to be consistent with the notations of [P5], we too will use this definition for the phase difference.

Figure 5 shows an array of N normal-metal tunnel junctions attached to a resistive electromagnetic environment R_e. This system can be described by the following Langevin equations [26]-[29]:

$$C_j\frac{\hbar\ddot{\varphi}_j}{2e} + \frac{1}{R_{T,j}}\frac{\hbar\dot{\varphi}_j}{2e} = \dot{q} + \tilde{\xi}_j, \qquad j = 1,\ldots,N;$$
$$V_x = \dot{q}R_e + \sum_{j=1}^{N}\frac{\hbar\dot{\varphi}}{2e} - \xi_e R_e. \tag{67}$$

The first one in Eqs. (67) is the analog of current equilibrium equation, Eq. (55), now extended to arrays of junctions, and the second one is the Ohm's law written in terms of voltage drops across the different elements of the circuit, V_j. The effective phase for the j-th junction is defined as $\varphi_j(t) \equiv \frac{2e}{\hbar}\int_0^t \mathrm{d}t' V_j(t')$. The shot noise of the j-th junction (and the shunt resistance R_e) is defined in a similar way to that of a simple tunnel junction in Eq.

(62),

$$\tilde{\xi}_j \equiv \xi_{1j} \cos\left(\frac{\varphi_j}{2}\right) + \xi_{2j} \sin\left(\frac{\varphi_j}{2}\right). \tag{68}$$

The Gaussian stochastic variables ξ_{kj} are given by the following correlators:

$$\begin{aligned}
&\langle \xi_{1j}(t_1)\xi_{1j}(t_2)\rangle = \langle \xi_{2j}(t_1)\xi_{2j}(t_2)\rangle = \frac{\mathcal{G}(t_1-t_2)}{R_j};\\
&\langle \xi_{1j}(t_1)\xi_{2j}(t_2)\rangle = 0; \quad \langle \xi_{\rm e}(t_1)\xi_{\rm e}(t_2)\rangle = \frac{\mathcal{G}(t_1-t_2)}{R_{\rm e}};\\
&\langle \xi_{1(2)i}(t_1)\xi_{1(2)j}\rangle = 0, \quad i \neq j.
\end{aligned} \tag{69}$$

Above, $\mathcal{G}(t)$ is defined as in Eq. (66). Notice that there is no correlation between the noises of different junctions.

The IV–curve of the array is given by averaging Eqs. (67) including the noise terms:

$$\begin{aligned}
I(V_{\rm x}) &= \langle \dot{q} \rangle = \frac{V}{R_\Sigma} - \sum_{j=1}^{N} \frac{R_{{\rm T},j}}{R_\Sigma} \langle \tilde{\xi}_j \rangle\\
V(V_{\rm x}) &= \left\langle \sum_{j=1}^{N} \frac{\hbar \dot{\varphi}_j}{2e} \right\rangle.
\end{aligned} \tag{70}$$

Here, $R_\Sigma \equiv \sum_{j=1}^{N} R_{{\rm T},j}$ is the total resistance of the array. The problem now reduces to the evaluation of average values $\langle \tilde{\xi}_j \rangle$. These values, in turn, are expressed in terms of the effective phases φ_j and their fluctuations $\delta\varphi_j \equiv \varphi_j - \langle \varphi_j \rangle$ by:

$$\begin{aligned}
\langle \tilde{\xi}_j \rangle &= \left\langle \xi_{1j} \cos\left(\frac{eV_j t}{\hbar} + \frac{\delta\varphi_j}{2}\right) + \xi_{2j} \sin\left(\frac{eV_j t}{\hbar} + \frac{\delta\varphi_j}{2}\right) \right\rangle\\
&\simeq \left\langle \left[\xi_{2j} \cos\left(\frac{eV_j t}{\hbar}\right) - \xi_{1j} \sin\left(\frac{eV_j t}{\hbar}\right)\right] \frac{\delta\varphi_j}{2} \right\rangle,
\end{aligned} \tag{71}$$

where $V_j \equiv \left\langle \frac{\hbar\dot{\varphi}_j}{2e} \right\rangle$ is the average voltage across the j-th junction†. To evaluate $\delta\varphi_j$, omitting $\dot{q}$ from Eqs. (67), one obtains for phases φ_j:

$$C_j \frac{\hbar\ddot{\varphi}_j}{2e} + \frac{1}{R_{{\rm T},j}} \frac{\hbar\dot{\varphi}_j}{2e} + \frac{1}{R_{\rm e}} \sum_{k=1}^{N} \frac{\hbar\dot{\varphi}_k}{2e} = \frac{V_{\rm x}}{R_{\rm e}} + \xi_{\rm e} + \tilde{\xi}_j. \tag{72}$$

† The angular brackets $\langle \ldots \rangle$ in Eq. (71) mean the averaging over the noises ξ_j. This averaging automatically includes the averaging with the density matrix and all other required averaging procedures. The nontrivial point is nonlinearity of the equations for the phases. The average values can easily be found only if the dependence of $\delta\varphi_j$ on all stochastic noises is linear. This is the case if one makes only one iteration. Generally, the solution of the problem cannot be exactly obtained.

Correspondingly, for an ideal bias voltage V_x, we find

$$C_j \frac{\hbar\delta\ddot{\varphi}_j}{2e} + \frac{1}{R_{Tj}} \frac{\hbar\delta\dot{\varphi}_j}{2e} + \frac{1}{R_e} \sum_{k=1}^{N} \frac{\hbar\delta\dot{\varphi}_k}{2e} = \xi_e + \delta\tilde{\xi}_j. \tag{73}$$

Applying the Fourier transformation, and solving for the equations thus obtained, one gets [30]:

$$\delta\varphi_j = \frac{2e}{\hbar} \int_{-\infty}^{t} \mathrm{d}t' K_j(t-t')\delta\tilde{\xi}_j(t') + \sum_{k\neq j} \frac{2e}{\hbar} \int_{-\infty}^{t} \mathrm{d}t' A_{kj}(t-t')\delta\tilde{\xi}_k(t'). \tag{74}$$

The response function, $K_j(t)$, is given by

$$K_j(t) \equiv \int_{-\infty}^{+\infty} \frac{\mathrm{d}\omega}{2\pi} \frac{Z_t^j(\omega)}{-i\omega + 0} \mathrm{e}^{-i\omega t}, \tag{75}$$

where $Z_t^j(\omega)$ is the total impedance of the array as seen by the j-th junction. The kernels $A_{kj}(t)$ are defined analogously. (Instead of $Z_t^j(\omega)$, there is a factor which relates the *ac* current injected into the k-th junction and the *ac* voltage measured across the j-th junction.) For a one–dimensional array, this impedance is

$$Z_t^j(\omega) = \frac{R_{T,j}}{1 - i\omega R_{T,j} C_j} \frac{R_e + \sum_{k\neq j} \frac{R_{T,k}}{1-i\omega R_{T,k} C_k}}{R_e + \sum_{k} \frac{R_{T,k}}{1-i\omega R_{T,k} C_k}}. \tag{76}$$

Obviously, Eqs. (73) and (74) should be solved iteratively. Within the first iteration $\delta\varphi_j = 0$ and, from Eq. (74),

$$\langle\tilde{\xi}_j\rangle = -\frac{2e}{\hbar R_{T,j}} \int_0^{\infty} \mathrm{d}t\, \mathcal{G}(t) K_j(t) \sin\left(\frac{eV_j t}{\hbar}\right). \tag{77}$$

Finally, for the current passing through the array, the generally valid expression (within the first iteration) can be derived as:

$$I = \frac{V}{R_\Sigma} + \frac{2e}{\hbar R_\Sigma} \int_0^{\infty} \mathrm{d}t\, \mathcal{G}(t) \Big[\sum_{j=1}^{N} K_j(t) \sin\left(\frac{eV_j t}{\hbar}\right) \Big]. \tag{78}$$

For a fully symmetric array with $R \equiv R_{T,j}$, $C \equiv C_j$, (and with negligible stray capacitances of the islands), the impedance $Z_t^j(\omega)$ takes the simpler form

$$Z_t^j(\omega) = \frac{R_e + (N-1)\frac{R_T}{1-i\omega R_T C}}{R_e\left(\frac{1}{R_T} - i\omega C\right) + N}, \tag{79}$$

and the response function, $K_j(t)$, becomes

$$K_j(t) = \frac{N-1}{N} R_T \left(1 - e^{-t/R_T C}\right) + \frac{R_e R_T}{N(R_e + N R_T)} \left(1 - e^{-\frac{R_e + N R_T}{R_e R_T C} t}\right). \tag{80}$$

Substituting for $Z_t^j(\omega)$ and $K_j(t)$ in Eq. (78)

$$I = \frac{k_B T v}{e R_T} - \frac{e k_B T}{\pi \hbar} \left[\frac{N-1}{N} F(v,u) + \frac{F(v,u_e)}{N(1 + N\frac{R_T}{R_e})} \right]. \tag{81}$$

Here $v \equiv eV/Nk_BT$, $u \equiv \hbar/2\pi k_B T R_T C$, $u_e \equiv u(1 + NR_T/R_e)$, and

$$F(v,u) \equiv v \left[\mathrm{Re}\Psi\left(1 + u - i\frac{v}{2\pi}\right) - \mathrm{Re}\Psi\left(1 - i\frac{v}{2\pi}\right) \right] - 2\pi u \, \mathrm{Im}\Psi\left(1 + u - i\frac{v}{2\pi}\right), \tag{82}$$

where $\Psi(x) \equiv \mathrm{d}[\ln \Gamma(x)]/\mathrm{d}x$ is the psi (or digamma) function. In the limit $T \to 0$ this expression reduces to that given in Ref. [28]. The differential conductance, $G \equiv \mathrm{d}I/\mathrm{d}V$, is now given by the expression

$$\frac{G}{G_\Sigma} = 1 - \frac{e^2 R_T}{\pi \hbar} \left[\frac{N-1}{N} \frac{\partial F(v,u)}{\partial v} + \frac{1}{N(1 + N\frac{R_T}{R_e})} \frac{\partial F(v,u_e)}{\partial v} \right]. \tag{83}$$

More theoretical details about the extension of the Langevin model to arrays of high–conductance tunnel junctions are given in [P5].

2.4 The Voltage Fluctuations Model

Besides all, more or less quantum –mechanical approaches presented above, a rather simple phenomenological classic model was put forward by Cleland *et al.* at an early stage in Ref. [32]. In this model, starting from the current–voltage (IV) characteristic of a tunnel junction which exhibits ideal Coulomb blockade, $I_{\mathrm{ideal}} \equiv \pm G_T(|V| - V_C)\Theta(|V| - V_C)$, the authors assume that the voltage fluctuations across the external impedance, δU, obey the normal distribution law

$$P(\delta U) \equiv \frac{1}{\sqrt{2\pi}} \frac{1}{\Delta U} \exp\left\{ -\left(\frac{\delta U}{2\Delta U}\right)^2 \right\}. \tag{84}$$

The IV–curve, then, is given by the convolution integral

$$I(V) = I_{\mathrm{ideal}}(V) * P(\delta U) \equiv \int_{-\infty}^{+\infty} \mathrm{d}(\delta U) I_{\mathrm{ideal}}(V + \delta V) P(\delta U). \tag{85}$$

Above, designating $\omega_c \equiv 1/R_T C$, the frequency–independent voltage fluctuation is obtained from the Johnson–Nyquist formula [13, 33] as a function of the cutoff frequency $\omega_{LC} \equiv 1/\sqrt{LC}$:

$$(\Delta U)^2 \equiv \left\langle \delta(U^2) \right\rangle = \frac{\hbar}{\pi} \int_0^{\omega_{LC}} \mathrm{d}\omega \mathrm{Re}[Z_e(\omega)]\omega = \frac{2\hbar\omega_c}{\pi C} \ln\left(\frac{\omega_{LC}}{\omega_c}\right). \tag{86}$$

Unfortunately because of its oversimplified assumptions, this model is not successful, and it fails to describe the measured data even qualitatively, as it will be shortly demonstrated in Chapter 3. That is why we do not detail it further.

Chapter 3:

RESULTS AND CONCLUSIONS

3.1 Review of the Basic Results in the Weak Tunneling Regime

A schematic view of a voltage biased N–junction array (without electromagnetic environment) is shown in Fig. 1 (c). The resistance of the i-th junction is denoted by $R_{\mathrm{T},i}$, and its capacitance by C_i. Each island has a stray capacitance $C_{0,i}$. In the weak Coulomb blockade regime, $\Delta_i \ll k_{\mathrm{B}}T$ [Δ_i is the Coulomb blockade threshold for the i-th junction] and in the stationary state, by series expansion of Eqs. (26)–(27), one gets for the differential conductance, G, of the array [34]:

$$\frac{G}{G_{\mathrm{T}}} = 1 - 2\sum_{i=1}^{N} \frac{R_{\mathrm{T},i}}{R_\Sigma}\,\frac{\Delta_i}{k_{\mathrm{B}}T}\, g\left(\frac{R_{\mathrm{T},i}}{R_\Sigma}\,\frac{eV}{k_{\mathrm{B}}T}\right). \tag{87}$$

Above $R_\Sigma \equiv \sum_{i=1}^{N} R_{\mathrm{T},i}$ is the total tunnel resistance of the array, G_{T} is the asymptotic value of the conductance G when $V \to \pm\infty$, and

$$g(x) \equiv \frac{x\sinh(x) - 4\sinh^2(x/2)}{8\sinh^4(x/2)} \tag{88}$$

is the g–function introduced in [18].

In a fully symmetric array with $R_{\mathrm{T}} \equiv R_{\mathrm{T},i}$, $C \equiv C_i$ and with negligible stray capacitance of each island $C_{0,i} \equiv 0$, Eq. (87) takes the simple form [34]:

$$G/G_{\mathrm{T}} \simeq 1 - u_N g(v_N). \tag{89}$$

Here $u_N \equiv 2[(N-1)/N](e^2/2Ck_{\mathrm{B}}T)$ and $v_N \equiv eV/Nk_{\mathrm{B}}T$. Against voltage, Eq. (89) represents a nearly bell–shaped dip of conductance. Within the first order in u_N, the half–width of this curve around small bias voltages, $V_{1/2,0}$, depends on the number of junctions

in the array, N, as:

$$V_{1/2,0} \simeq 5.439 \frac{N k_{\rm B}}{e} T. \tag{90}$$

This relation is of fundamental importance in the Coulomb blockade thermometry (CBT) and it can be used as a primary measure to determine temperature. Correspondingly, for the conductance drop at zero bias voltage, one finds

$$\frac{\Delta G}{G_{\rm T}} \simeq \frac{1}{6} u_N. \tag{91}$$

This equation, too, can be used for evaluation of temperature, but now one should know the value of junction capacitances C, *i.e.*, this expression has a secondary nature.

More accurate relation for the conductance of a fully symmetric array can be obtained by taking the higher order terms in the high temperature expansion ($u_N \ll 1$) in Eq. (89):

$$\begin{aligned} G/G_{\rm T} = 1 - u_N g(v_N) - \frac{1}{4} u_N^2 [\, g''(v_N) h(v_N) + g'(v_N) h'(v_N)] \\ - \frac{1}{8} u_N^3 [\, \frac{1}{4} g''''(v_N) h(v_N)^2 + \frac{1}{3} g''(v_N) + \frac{1}{2} g'''(v_N) h'(v_N) h(v_N)] - \cdots, \end{aligned} \tag{92}$$

where $h(x) \equiv x \coth(x/2)$ and $v_N \equiv eV_{1/2,0}/2k_{\rm B}T$. Using this expression, one can derive the correction to the full–width at half–minimum, $\Delta V_{1/2} \equiv V_{1/2} - V_{1/2,0}$, in Eq. (90) as:

$$\frac{\Delta V_{1/2}}{V_{1/2,0}} \simeq 0.39211 \frac{\Delta G}{G_{\rm T}}. \tag{93}$$

Similarly, the correction to the conductance dip beyond Eq. (91) is given by:

$$\frac{\Delta G}{G_{\rm T}} = \frac{1}{6} u_N - \frac{1}{60} u_N^2 + \frac{1}{630} u_N^3 + \cdots. \tag{94}$$

The effect of these corrections, Eqs. (93) and (94), is to broaden and to flatten the conductance dip, respectively.

3.2 Single Tunnel Junctions

In a tunnel system without any intentional environment, the impedance of the external circuit is of the order of free space impedance $Z_0 \equiv \sqrt{\mu_0/\epsilon_0} \simeq 377\ \Omega$. This value is much smaller than that of quantum resistance, $R_{\rm K} \simeq 25.8\ {\rm k}\Omega$. Since the charging effects in single

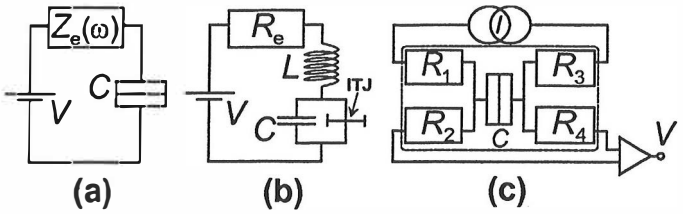

FIG. 6: **(a)** A tunnel junction connected through an external impedance $Z_e(\omega)$ to the voltage source which is equal to V if $R_T \gg |Z_e(\omega)|$, **(b)** The impedance seen by the ideal tunnel junction (ITJ) in the resistive environment R_e in series with the line inductance L providing the high–frequency cutoff, and **(c)** The four–probe configuration of the samples with on–chip resistances R_j.

tunnel junctions are incorporated to the non-zero impedance of the electromagnetic environment in the vicinity of the junction [3, 6], one may expect that these effects become more pronounced if the on–chip impedance in the vicinity of the junction becomes comparable to R_K. The motivation for performing the experiments outlined below, and for involving different theoretical models, has been to examine this pre–assumption.

Samples with well-defined resistive environment were made by three–angle evaporation techniques. The tunnel structures were obtained by overlap of aluminum films with oxide barrier in between. Typical area of tunnel junctions was about (0.1×0.1) μm^2. Environmental resistances in the range 1–20 kΩ were obtained by evaporation of about 100 nm wide, 2 μm long, and 3–8 nm thick chromium films into the vicinity ($\sim$ 1 μm) of the junction. The inductance of thin films was estimated using the simple expression $L \simeq (\mu l/2\pi)\ln(w/t)$. Here l, w and t are the length, width and thickness of the thin film leads connected to the junction, respectively. With $l \simeq 2$ μm, $t \simeq 0.1$–1 μm, $w \simeq 0.1$–1 mm, and $\mu \simeq \mu_0$ (μ_0 is the vacuum permeability), one gets $L \simeq 4$ pH. The resistance of each chromium lead [Fig. 6 (c)], R_j, was estimated by a linear fit to its measured current–voltage (IV) characteristic. The measured IV–curves were linear within much better than 5 % over the range of conductance measurements. The resistance of environment R_e, thus, was obtained as $R_e = R_1R_2/(R_1 + R_2) + R_3R_4/(R_3 + R_4)$. All measurements were performed by lock–in techniques in a four–probe configuration. Samples were cooled down in a home–made dilu-

Sample	1	2	3	4	5	6	7	8
α_t	3.02	0.029	3.10	0.076	0.69	1.30	5.86	1.04
α_e	1.50	2.80	7.59	7.82	8.06	16.33	20.32	8.09
C (fF)	0.92	0.45	1.02	0.63	1.07	1.17	1.99	1.25

TABLE I: Parameters of the measured samples. Here, $\alpha_t \equiv R_K/R_T$ and $\alpha_e \equiv R_K/R_e$.

tion refrigerator. To suppress superconductivity of the aluminum samples below $T \simeq 1.2$ K, a permanent magnet attached to the sample holder with a field of about 1–2 T was used.

Eight samples with different tunneling strengths, $\alpha_t \equiv R_K/R_T$, and with various environmental resistances, $\alpha_e \equiv R_K/R_e$, were measured. The parameters of these samples are collected into Table I. Samples were chosen to have almost the same capacitances of about 1 fF. This makes the comparison of measured data more reliable.

The differential conductance of the samples was measured at different temperatures. Furthermore, to make comparison between different data, the (inverse) normalized conductance drop at zero bias voltage, $(\Delta G/G_T)^{-1}$, was evaluated as a function of temperature $[\Delta G \equiv G_T - G(V = 0)]$. The advantage of this choice is that this dependence, down to not very low temperatures, is not affected by heating due to bias. Especially, for samples in the strong tunneling regime with $\alpha_t \gtrsim 1$, the conductance dip, ΔG, is a better measure of comparison than the half–width of this curve, $V_{1/2}$, around zero bias voltage. Due to higher current the heating effects are more pronounced for high–conductance tunnel junctions and this, in turn, can affect the half–width of the conductance curve [18]. Also an important parameter which can be involved in comparisons between the predictions of different theories and between various measured data, is the offset of the fitted straight line, δ, to the measured data $(T, G_T/\Delta G)$. Such fits are depicted in Figs. 7 and 8. Figures 9 and 10 show the measured data for a sample with $R_T = 24.9$ kΩ, $R_e = 3.19$ kΩ and $C = 1.3$ fF (sample 8), at $T = 4.2$ K and at $T \simeq 50$ mK. The capacitances of the samples were estimated by finding the best fit to the measured conductance curves at $T = 4.2$ K using Eqs. (18)–(20). In fact, this is a way for evaluation of junction capacitance [18].

Let us start our comparison to the theories involved with the voltage fluctuation (VF)

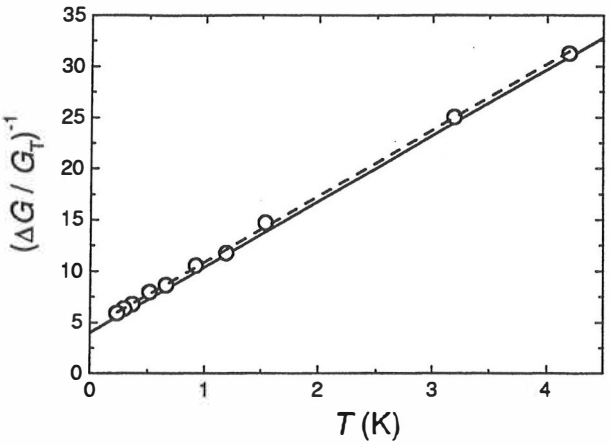

FIG. 7: Inverse depth of the normalized conductance dip measured at different temperatures for sample 7 (see Table I). The solid line stands for the result of the basic $P(E)$ theory, whereas the dashed line incorporates the strong tunneling correction (the extended $P(E)$ theory). The Ohmic approximation of the environment (MF1) and the full iteration (MFn) fall on the same line.

model [32]. Using Eqs. (85)–(86), the differential conductance can be found numerically, $V_C/\Delta U$ being the only parameter. For our samples $L \sim 10$ pH. The value of cutoff frequency, $\omega_c = 1/\sqrt{LC}$, for sample 8 in Table I can be obtained by putting $C = 1.3$ fF, the fitting parameter, $V_C/\Delta U$, being equal to 0.28. The corresponding curve at $T = 0$ is shown in Fig. 10 (the dashed line). Clearly, this model fails to reproduce the observed data. The disagreement between theory and experiment becomes even worse if thermal fluctuations are not supposed to be negligibly small.

Next, let us consider the phase-correlation theory, and its extension to the strong tunneling regime.

The main parameters in obtaining numerical fits to the conductance curves were $\alpha_e \equiv R_e/R_K$ and $\Omega_c \equiv \hbar\omega_c/k_BT$ [$\omega_c \equiv 1/R_eC$]. As a starting point for finding the best theoretical fits to the conductance curves, one may use the simple relation between the conductance

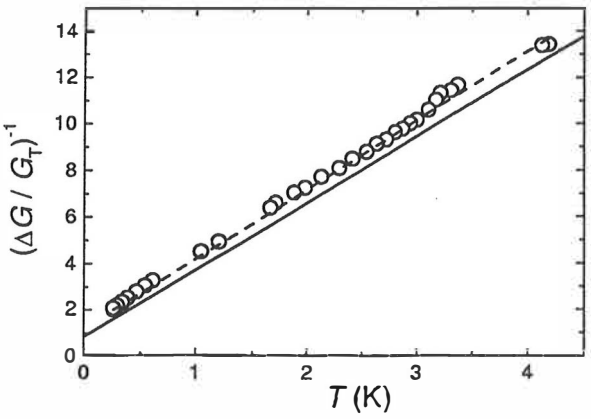

FIG. 8: The same as in Fig 7, but now for the sample 1 of Table I.

dip and the capacitance of the junction derived in [18]:

$$\frac{\Delta G}{G_T} \simeq \frac{e^2}{6C} \frac{1}{k_B T}. \tag{95}$$

The capacitance values obtained this way are generally consistent with those estimated from the width of the Coulomb gap, $\Delta V = e/C$, in the IV-characteristics of the junctions measured at low temperature. However, the use of conductance curve for evaluation of C is advantageous to that derived from the IV-curve, since the former one gives more reliable values even at higher temperatures. Temperatures were measured by a resistor thermometer calibrated against the CBT sensors, $T \simeq 50$ mK. This is in reasonable agreement with the value $T \simeq 70$ mK predicted by the $P(E)$ theory (solid line in Fig. 10), and with the temperature given by the simple linear relation in Eq. (90).

The difference between the refrigerator temperature and that obtained from the numerical fit to the measured conductance curve [cf. Eq. (90), too] was not specific to the sample presented in Figs. 9 and 10, but for the rest of the samples as well. In all of the samples, the zero-bias conductance saturated to a value corresponding to $T > 60$ mK, even when the refrigerator temperature was as low as ~ 40 mK. This difference can be caused *hot electron effects* [35], according to which, the phonon and the electron temperatures in the substrate and the junction itself, respectively, are not necessarily the same. In a voltage-biased tunnel

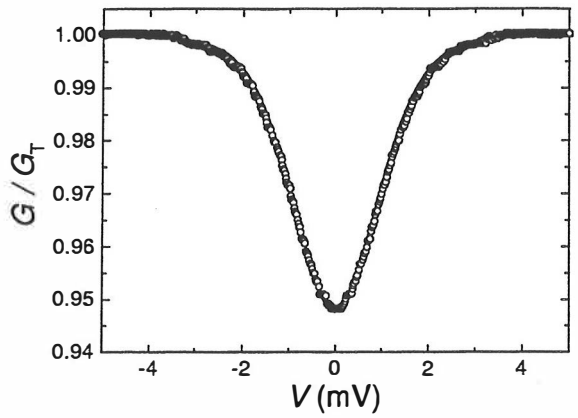

FIG. 9: The differential conductance measured at $T = 4.2$ K (open circles) for sample 8 in Table I. The solid curve is the best fit obtained from the phase–correlation theory. The fitting parameter was $\Omega_c = 0.45$ [$\Omega_c \equiv \hbar/(R_e C k_B T)$].

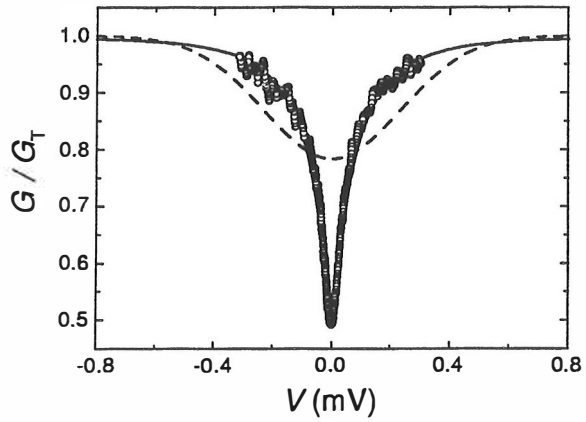

FIG. 10: Measured differential conductance of sample 8 at $T \simeq 50$ mK (open circles), together with the prediction of the voltage fluctuation (VF) model at $T = 0$ (dashed line). The solid line has been obtained from $P(E)$ theory with the fitting parameter $\Omega_c = 27$, which corresponds to $T = 70$ mK (cf. Fig. 9).

junction (or a system of junctions, as well) the heat produced in the junction is equal to V^2/R_T. Due to high thermal resistance of tunnel junction systems, this heat can hardly be transported through the junction(s); instead it leaks out to the substrate causing the excitation of phonons there [35]. That is why, one may expect that at $T \sim 100$ mK the substrate temperature, *i.e.* the refrigerator temperature, should *all* the time be somewhat lower than the temperature in the tunnel system itself.

In what follows, we will study the samples in the strong tunneling regime, *i.e.* the samples with $\alpha_t \gtrsim 1$. To this end, the phase–correlation theory together with the path–integral approach will be involved.

The zero–bias conductance in the tunneling channel model, *i.e.* in the extended $P(E)$ theory, can be derived from Eq. (38). Practically, this equation can be solved, with good accuracy, within only a few iterations. Further iterations account for the non–linearity of the environment originating from the tunnel element [11].

To see how this model and the path–integral approach improve the agreement between the measured data and the theoretical predictions for the high–conductance samples, one first notices that in the high–temperature limit, $k_B T \gg E_C$, irrespective of the strength of tunneling (weak or strong), dependence between the (inverse) conductance dip and the temperature obeys a linear form, Eqs. (51) and (52).

The offset, δ, in the strong tunneling regime, Eq. (52), depends on *both* α_e and α_t, but not on the capacitance of the tunnel junction. (In fact, the dependence of the offset on the strength of tunneling, α_t, can further be confirmed by the other techniques, too, as will be discussed in respect of the quasiclassical Langevin model.) The analytical form of δ for the extended $P(E)$ theory has not been derived; therefore we only present the data evaluated from a numerical solution of Eq. (38) in Figs. 11 and 12. The path–integral method does not give considerable improvement over the prediction of the basic phase–correlation theory (open circles in Fig. 12). Instead, the extended $P(E)$ theory reduces the discrepancy between the theory and the experiment perceivably (solid triangles). Especially, one should pay attention to the fact that the larger α_t, the better the agreement between the measured and the predicted data becomes. More evidence in favor of the superiority of the channel

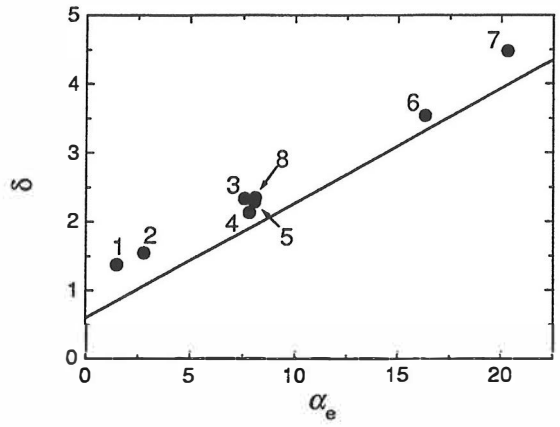

FIG. 11: The measured offsets of the samples in Table I as a function of α_e. The solid line is the prediction of the phase–correlation theory in the weak tunneling regime.

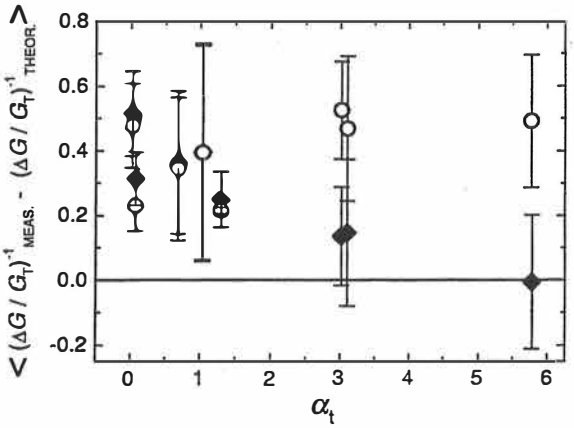

FIG. 12: The mean difference of the inverse (normalized) conductance curve, $(\Delta G/G_T)^{-1}$, from its theoretical prediction. The angular brackets denote the average over the measured values at different temperatures. The open circles are for the basic $P(E)$ theory, and the solid diamonds for the extended $P(E)$ theory. The latter takes the strong tunneling corrections into account.

model is demonstrated in Figs. 7 and 8. Also, as can be seen from the latter figure, while solving for the above equations self–consistently, the number of iterations does not matter, which in turn implicates that the contribution of tunnel element to the electromagnetic environment is almost linear. However, at lower temperatures the non–linear contribution of the junction admittance is not negligible [11], and one needs more iterations.

3.3 Tunnel Junction Arrays

While study of single tunnel junctions is of more fundamental nature, tunnel junction arrays, like single electron transistor and Coulomb blockade thermometer (CBT), are of more interest in practical applications. CBT was invented in 1994 at the University of Jyväskylä, and since then, it has been developed to a commercial product. The basic idea in this thermometer is that the full–width at half–minimum of conductance curve, $V_{1/2}$, has a simple dependence on temperature, Eq. (90). Originally, this relation was obtained in the high–temperature limit and for vanishing environmental resistance. Recently, it has also been derived by the quasiclassical Langevin equation approach [P5]. Different aspects of CBT thermometry and the effect of various factors on it, such as inhomogeneity of the junctions, tolerance to magnetic field, reduction of immunity to background charges, influence of neutron radiation, the hot electron effects, temperature range limitation and how to overcome them, as well as higher–order theoretical corrections to the simple linear relation, Eq. (90), were already studied in a systematic way by the beginning of this work [18, 36]. One of our main motivations to investigate tunnel junction arrays influenced by the electromagnetic environment was to complete our picture of CBT. Furthermore, by the time, such effects were never studied in an extensive manner. Besides this practical importance, by the increasing interest in the utilization of (superconducting) tunnel junction arrays as building blocks of quantum bits (QBIT's), the role of dissipation in such systems is of interest. For instance, one of the key points in the realization of (superconducting) QBIT's is the understanding of (de)coherence in electronic quantum systems. This, in turn, is in close relation with the role of dissipation in such structures.

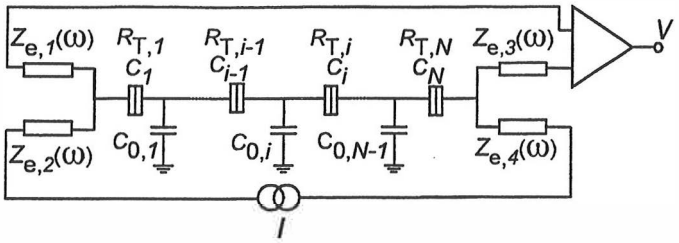

FIG. 13: Schematic of an N–junction array in an electromagnetic environment. For a purely resistive environment $Z_{e,j}(\omega) = R_j$.

3.3.1 One–dimensional Arrays of Low–conductance Tunnel Junctions

With low–conductance array we mean an array in which the per–junction asymptotic resistance (tunnel junction resistance at large bias voltages) of the array, $R_{T,k}$, is greater than the quantum resistance R_K. All the time, it is assumed that the arrays are homogeneous, *i.e.* tunnel junctions in the arrays have the same value of asymptotic resistances $R_T \equiv R_{T,k}$, and the same per–junction capacitances $C \equiv C_k$. In addition, it is supposed that the stray capacitance of each island, $C_{0,k}$, is negligible.† All of these assumptions are well justified, and they do not alter the conclusions made here noticeably. Instead, they make numerical calculations, especially Monte–Carlo simulations, more feasible.

A schematic view of the samples is shown in Fig. 13. Typically, we made samples with a pair of arrays each consisting of different number of junctions, *e.g.* arrays with $N = 1, 2$; $N = 2, 8$; and $N = 2, 20$. This way, the consistency of the results was ensured, and the intercomparison of results for different arrays was made more reliable. The distance between arrays of each pair was 3 μm. The Al/AlO_x/Al tunnel junctions had an area of about 0.01–0.05 μm^2. To provide a well–defined environment, four chromium resistors, $Z_{e,j}(\omega) \equiv R_j$, two at each end (Fig. 13) were made at a distance of about 2 μm from the terminal junctions of the array. The length, width and thickness of chromium films was about 2 μm, 100 nm,

† For the k-th island of length l and made over a material with permittivity ϵ, the stray capacitance, $C_{0,k}$, can be written as $C_{0,k} \sim \epsilon l$. In our samples islands are made of aluminum and their lengths are ~ 1 μm. This gives rise to $C_{0,k} \sim 0.5 \times 10^{-17}$ F. This is two order of magnitudes smaller than typical capacitances of our samples ($\sim 2 - 5$ fF). This is why we neglect stray capacitances now.

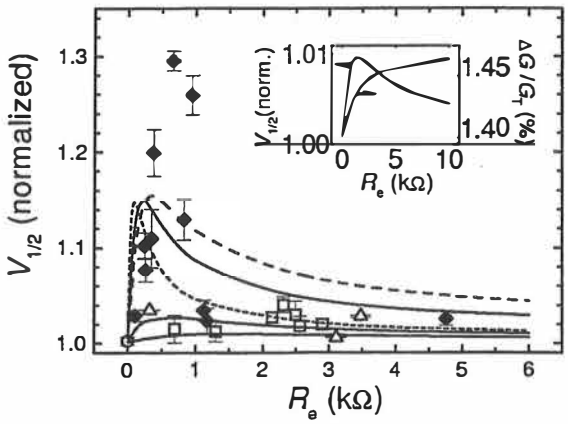

FIG. 14: Measured half–width of the conductance curve, normalized by $V_{1/2,0} = 5.439Nk_BT/e$ versus the on–chip external resistance for samples with $N = 2$ (solid diamonds), $N = 8$ (open triangles), and $N = 20$ (open squares). The lowermost solid curve is the result of a Monte–Carlo simulation for a completely symmetric 20–junction array with $C \equiv C_k = 5.0$ fF. The uppermost solid curve is the result of simulation for a double–junction array with $C = 2.2$ fF, whereas the dotted and the dashed curves correspond to $C = 5.0$ fF and $C = 1.4$ fF, respectively. The middle solid line is the result of simulation for an array with $N = 8$ and $C = 5.0$ fF. The inset shows the normalized half–width together with the depth of the conductance curve, obtained from theory, for a 20–junction array.

and 3–8 nm, respectively. All measurements were carried out at $T \simeq 4.2$ K.

The electric current through the array was calculated by use of Eqs. (26)–(28), and as described in Section 2.2.

In the case of a completely symmetric array and a purely resistive environment, $Z_e(\omega) = R_e$, the phase–phase correlation function, $J(t) \equiv J_k(t)$, can also be analytically evaluated by partial sum expansion of $\coth(x)$ in Eq. (27), resulting in:

$$J(t) = \frac{\pi}{N^2}\frac{R_e}{R_K}\left\{(1-e^{-|N\omega_c t|})[\cot(\frac{N\hbar\omega_c}{2k_BT})-i]-\frac{2|t\,|}{\beta\hbar}+4\sum_{m=1}^{\infty}\frac{(N\omega_c)^2(1-e^{-|N\omega_m t|})}{2\pi l[\omega_m{}^2-(N\omega_c)^2]}\right\}. \quad (96)$$

Above, $\omega_c \equiv 1/R_eC$ is the cutoff frequency of the R_eC–circuit, and $\omega_m = 2\pi m/\beta\hbar$ are Matsubara frequencies.

For a symmetric two-junction array, the current can be calculated by a different method, too. Here, one obtains the probability distribution, $\sigma(\{n\})$, of finding n excess electrons on the island between tunnel junctions, after which the equilibrium current through the array, $I \equiv I_k$, can be derived by use of Eq. (6). The algorithm utilized in evaluation of $\sigma(n)$'s is detailed in [8]. In practice, especially at not very high temperatures, the summation above runs over a very limited number of states, typically $n \leq 10$. With such a choice of n, the IV–curve can be derived within several minutes. Instead, while using the Monte–Carlo method, the simulations may take several hours. This depends on the number of (pseudo)random tunneling events simulated in the numerical calculations [37].

3.3.2 One–dimensional Arrays of High–conductance Tunnel Junctions

In what follows, the measured data for high–conductance arrays, together with their comparison to the predictions of the Langevin equation approach introduced in Section 2.3.3, will be presented.

Homogeneous tunnel junction arrays with high conductances, *i.e.* arrays with per-junction resistances $R_T \equiv R_{T,j}$ (and $C \equiv C_j$) smaller than that of the quantum resistance, $R_T \ll R_K$, were made by conventional shadow technique. The number of junctions in the array, N, was twenty, and each junction had an area of about 0.025 μm^2. Typical per-junction resistance of the arrays was 1–2 kΩ. Furthermore, for comparison, we made two additional samples with higher (per-junction) resistances, *i.e.* with resistances equal to 20 and 23 kΩ. As was already pointed out, the heating effects have considerable role in the samples with lower resistances. To decrease these effects at higher bias voltages, the islands between junctions in the studied samples were made sufficiently large and, in some cases, the cooling bars (see, *e.g.*, [P1]) were attached to these islands. The samples were measured in the liquid helium temperature range 1.5 K $\lesssim T \lesssim$ 4.5 K. To measure the temperature accurately enough, the readings of vapor pressure of helium as well as those of CBT sensors made in the vicinity of the sample to be measured were simultaneously recorded.

Next, let us have a closer look at the predictions of the quasiclassical approach in terms of

the resistance enhancement at zero bias voltage, $\Delta R \equiv R(V=0) - R_{\rm T}$. The reason simply is that the dependence of $R_{\rm T}/\Delta R$ on temperature turns out to have (both theoretically and experimentally), to a good extent, a linear form. This makes the comparison between the theory and the measured data more straightforward. To this end, one should re-express the generally valid relation for the IV–curve of a homogeneous high–conductance array, Eq. (81), in a form suitable for samples investigated here, *i.e.* for an array in the high temperature regime $u \ll 1$ [$u \equiv \hbar/2\pi k_{\rm B}TR_{\rm T}C$, and $\frac{u}{u_N} = \frac{1}{(2\pi)^2}\frac{N}{N-1}\frac{R_{\rm K}}{R_{\rm T}}$], and with negligible environmental resistance, $R_{\rm e} = 0$.

Putting $R_{\rm e} = 0$ in Eq. (81), and considering the low temperature regime, $u \ll 1$, within the fist order in u, one gets

$$\begin{aligned} I &= \frac{k_{\rm B}Tv}{eR_{\rm T}} - \frac{N-1}{N}\frac{ek_{\rm B}T}{\pi\hbar}u\left[v\,{\rm Re}\Psi'\left(1-i\frac{v}{2\pi}\right) - 2\pi\,{\rm Im}\Psi\left(1-i\frac{v}{2\pi}\right)\right] \\ &= \frac{k_{\rm B}Tv}{eR_{\rm T}} - \frac{N-1}{2N}\frac{e}{R_{\rm T}C}\left[\coth\left(\frac{v}{2}\right) - \frac{v}{2\sinh^2\left(\frac{v}{2}\right)}\right], \end{aligned} \tag{97}$$

where $v \equiv eV/Nk_{\rm B}T$. The differential conductance, then, is

$$\frac{1}{G_\Sigma}\frac{{\rm d}I}{{\rm d}V} = 1 - \frac{N-1}{N}\frac{e^2}{Ck_BT}\frac{v\sinh(v) - 4\sinh^2\left(\frac{v}{2}\right)}{8\sinh^4\left(\frac{v}{2}\right)}. \tag{98}$$

Here, $G_\Sigma \equiv 1/R_\Sigma$ and $R_\Sigma \equiv \sum_{j=1}^{N} R_{{\rm T},j}$ is the total resistance of the array. This is identical to Eq. (89) already obtained for the junction arrays in the weak tunneling regime [18]. From Eq. (98), one can easily derive the familiar linear relation: $V_{1/2,0} = 5.439Nk_{\rm B}T/e$. However, to go beyond the linear approximation, and to find the necessary correction to this formula in the high temperature limit (for high–conductance arrays), we consider an array with negligible environmental resistance, $R_{\rm e} = 0$ in Eq. (81), and numerically solve the resulting equation

$$\frac{\partial F(v_{1/2}/2, u)}{\partial v} = \frac{1}{2}\frac{\partial F(0,u)}{\partial v}. \tag{99}$$

Here $v_{1/2}$ is the normalized half–width, $v_{1/2} \equiv V_{1/2}/V_{1/2,0}$. The solution to this equation is plotted in Fig. 15. Analytically, Eq. (81) can be expressed in terms of u as:

$$v_{1/2} = 1 + 0.704u - 0.24u^2 + 0.082u^3 + \mathcal{O}(u^4). \tag{100}$$

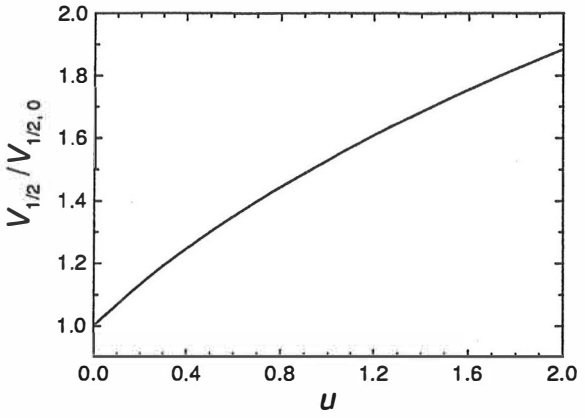

FIG. 15: The normalized half–width of the conductance dip at zero bias voltage as a function of (inverse) temperature $u \equiv \hbar/[2\pi k_B T R_T C]$. At higher temperatures the curve is almost linear in u [cf. Eq. (99)].

The accuracy of expression above is about 1% for $u \leq 1$ and 0.1% for $u \leq 1/3$. This is in agreement with the exact numerical solution shown in the figure: at higher temperatures the curve is linear in u. The general expression for the zero bias conductance, $G_0 \equiv G(V=0)$, can be obtained from Eq. (83):

$$\frac{G_0}{G_\Sigma} = 1 - \frac{N-1}{N}\frac{e^2 R_T}{\pi\hbar}\Big\{\Psi(1+u) + \gamma + u\,\Psi'(1+u)\Big\}. \tag{101}$$

Here, $\gamma \simeq 0.577$ is the Euler's constant [16]. In the high temperature limit, this equation takes the form

$$\begin{aligned}\frac{G_0}{G_\Sigma} &= 1 - \frac{N-1}{N}\frac{e^2 R_T}{\pi\hbar}\left\{\frac{\pi^2}{3}u - 3\zeta(3)u^2 + \cdots\right\} \\ &\equiv 1 - \frac{N-1}{N}\frac{E_C}{3k_B T} + A\frac{E_C^2}{(k_B T)^2} + \cdots.\end{aligned} \tag{102}$$

Above, $E_C \equiv e^2/2C$ is the "per-junction" charging energy, $A = A_{\rm strong} \equiv \frac{N-1}{N}\frac{3\zeta(3)}{2\pi^4}\frac{R_K}{R}$, and $\zeta(x)$ is the zeta function [16]. This equation is very similar to that derived for an array of low–conductance tunnel junctions and in the weak tunneling regime: $A = A_{\rm weak} \equiv \frac{1}{15}\left(\frac{N-1}{N}\right)^2$ [18].

In practice, most of the arrays have per-junction resistances close to that of quantum resistance R_K. The reason is that in applications, like in the CBT thermometry, arrays with large resistance are difficult to measure, and those with very small resistances are subject to non–desirable heating effects. For arrays with $R_{T,j} \simeq R_K$, *i.e.* for arrays in the *intermediate regime*, one can conjecture that $A = A_{strong} + A_{weak}$. This assumption has already been proved for a single electron transistor in the high temperature limit $u \equiv \hbar/2\pi k_B T R_T C \ll 1$ [31], and, since there is not any qualitative difference between the short and the long arrays, one may expect that it is valid for long arrays as well. Indeed, the experimental data, to be discussed in the following lines, gives more support in favor of this assumption.

Within the first order in u, the inverse resistance enhancement at zero bias voltage, $R_T/\Delta R$, can be easily derived from Eq. (102) as:

$$\frac{R_T}{\Delta R} = 3\frac{N}{N-1}\frac{k_B}{E_C}T + a\frac{R_K}{R_T} + b, \tag{103}$$

where, according to the theory,

$$a \equiv \frac{N}{N-1}\frac{27\zeta(3)}{2\pi^4} \simeq 0.175 \tag{104}$$

and

$$b \equiv \begin{cases} -1, & A = A_{strong}; \\ -2/5, & A = A_{strong} + A_{weak}. \end{cases} \tag{105}$$

Equation (103) is linear in T, and its slope depends on the capacitance of the junctions in the array. Indeed, this fact can be utilized in the estimation of junction capacitances. Furthermore, the *offset* of this line, *i.e.* the value of (inverse) resistance enhancement at very low temperatures, depends on the number of junctions in the array, N, and on the tunneling regime, *i.e.* on the ratio of quantum and per-junction resistances R_K/R_T. The latter one is a pure strong tunneling effect, and it modifies the similar relation already derived for the arrays in the weak tunneling regime [18].

Figure 16 shows the temperature dependence of the zero bias voltage anomaly, $R_T/\Delta R$, for two samples in the high–conductance regime. The number of junctions in each array was $N = 20$, and the samples had asymptotic (per-junction) resistances of 23 kΩ (open circles)

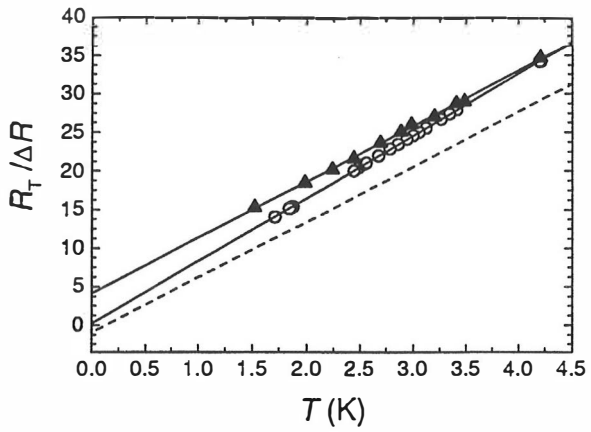

FIG. 16: The temperature dependence of the zero bias voltage anomaly, $R_T/\Delta R$, for two arrays with per-junction resistances of 1.2 kΩ and 23 kΩ (solid triangles and open circuits, respectively). The solid lines are linear fits to the experimental data. The dashed line is the prediction of Monte-Carlo simulation based on the (basic) phase–correlation theory for the sample with $R_T = 1.2$ kΩ.

and 1.2 kΩ (solid triangles). The solid lines are linear fits to the measured data. By fitting the slope of these curves to Eq. (103), one finds $C = 2.4$ fF and $C = 2.1$ fF for arrays with $R_T = 23$ kΩ (open circles) and $R_T = 1.2$ kΩ (solid triangles).

The offset values obtained from the linear fits to the measured data (solid lines in Fig. 16) are 4.1 and 0.2 for the samples represented by the solid triangles and the open circles, respectively. The corresponding values, obtained from Eq. (103), are 3.4 and -0.2. These values are not in a perfect agreement with the measured ones, but they show improvement over the prediction of the weak tunneling theory, where the value of the offset is all the time, irrespective of the strength of tunneling R_K/R_T, equal to -2/5. Furthermore, to make an overall comparison between the predictions of the phase-correlation theory (developed for the weak tunneling regime) and those of the model presented here, the results of Monte-Carlo simulations based on the $P(E)$ theory are shown by a dashed line in Fig. 16. Clearly, the quasiclassical model improves the agreement between the theory and the measurement. The only fitting parameter in Monte-Carlo simulations has been the capacitance of the

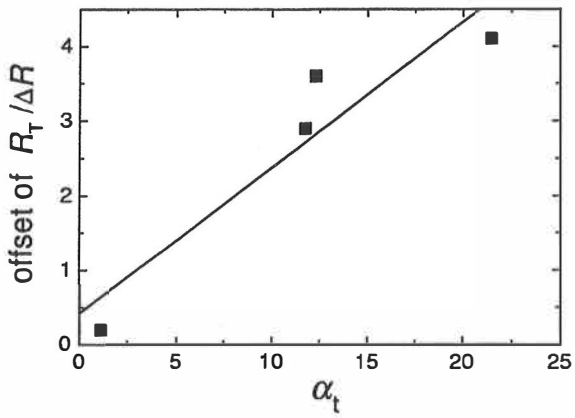

FIG. 17: The dependence of the offset of $R_T/\Delta R$ (cf. Fig. 16) on the dimensionless resistance of the junctions, $\alpha_t \equiv R_K/R_T$. The measured data are shown by squares, the solid line is the best linear fit [cf. Eq. (103)].

junctions. By comparison of the measured conductance curves of the array represented by the solid triangles to those obtained from the numerical simulations, we obtained the value $C = 2.1$ fF for the capacitance. Notice that this value is in excellent agreement with that derived from Eq. (103). [We also checked for the effect of the electromagnetic environment on the offset and observed that it has a vanishingly small influence on the offset value. The dashed line in Fig. 16 has been obtained with negligible environmental resistance.] It is also noticeable that the disagreement between the theoretical (dashed line) and the extrapolated measured offset for the sample with $R_T = 23$ kΩ (lower solid line) is much smaller. This is quite understandable: the sample represented by the open circles belongs to the intermediate tunneling regime, where the phase-correlation theory should work properly.

The offset values for two additional samples with $R_T = 2.1$ kΩ and $R_T = 2.2$ kΩ were equal to 3.6 and 2.9, respectively. The corresponding theoretical predictions are 1.8 and 1.2. Figure 17 shows the measured offset values (solid squares) as a function of tunneling strength for different samples. The solid line is the best linear fit with $a = 0.19 \pm 0.05$ and $b = 0.4 \pm 0.7$. The value of a is in agreement with that of Eq. (104), whereas the

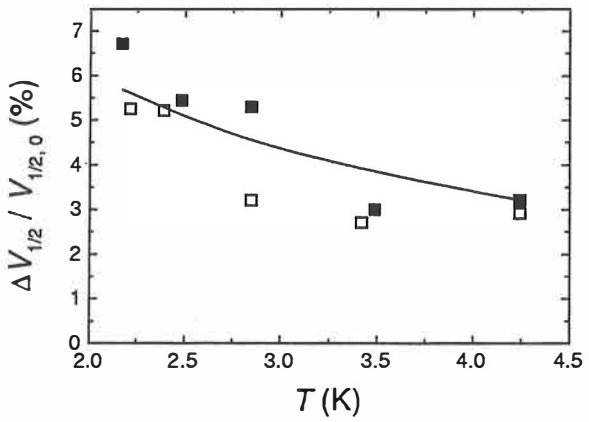

FIG. 18: The measured temperature dependence of the normalized half–width $\Delta V_{1/2}/V_{1/2,0}$ for two arrays (solid and open squares) with the same per-junction resistances $R_T = 2.1$ kΩ. The solid curve has been obtained from the strong tunneling theory (see the text).

values of b obtained from the fit to the measured data differs largely from those given by Eq. (105). We have checked for the influence of the electromagnetic environment as well as for the inhomogeneity effects. These effects do not improve the agreement between the two different values for b; therefore the reason for this discrepancy remains unclear.

Obviously, samples with lower (per-junction) resistances show larger offsets. The scatter of the measured offset around the linear fit (±0.5) could be attributed to the inhomogeneity of the arrays (otherwise the samples with $R_T = 2.1$ kΩ and $R_T = 2.2$ kΩ should have the same offset values). For instance, a 20 % fluctuation of the per-junction resistance, $R_{T,j}$, around the mean value, R_T, is enough to explain the observed discrepancy. A reasonable explanation for this fluctuation, instead, could be a 40 % variation in the areas of the "odd" and the "even" tunnel junctions in the two–angle evaporation process, which, however, seems larger than expected.

The variation of the normalized half–width, $\Delta V_{1/2}/V_{1/2,0}$, as a function of temperature for two 20–junction arrays, both with $R_T = 2.1$ kΩ, is shown in Fig. 18 [$\Delta V_{1/2} \equiv V_{1/2} - V_{1/2,0}$]. The solid curve is the prediction of Eq. (100).

From Eqs. (100) and (102), a useful relation between the deviation of the normalized half–width, $\Delta V_{1/2}/V_{1/2,0}$, and that of the depth of the normalized conductance dip, $\Delta G/G_\Sigma$ [$\Delta G \equiv G_\Sigma - G(V=0)$], can be obtained:

$$\frac{\Delta V_{1/2}}{V_{1/2,0}} = \chi(R_K/R_T)\frac{\Delta G}{G_\Sigma}. \tag{106}$$

In the strong tunneling regime

$$\chi(R_K/R_T) \simeq 0.108\frac{N}{N-1}\frac{R_K}{R_T}. \tag{107}$$

This relation is reminiscent of that already derived for arrays in the weak tunneling regime, Eq. (93):

$$\chi(R_K/R_T) \simeq 0.392. \tag{108}$$

In the intermediate regime, as was the case with the value of A in Eqs. (103)–(105), one may conjecture that $\chi(R_K/R_T)$ is the sum of Eqs. (107) and (108). The experimental data, to be presented below, support this assumption.

Table II shows the measured data for five different samples together with the corresponding theoretical predictions. The temperature in measurements was $T \simeq 4.2$ K and its exact value was obtained from the vapor pressure of liquid helium. In the table, $V_{1/2,\text{meas.}}$ stands for the value of the half–width obtained *directly* from the measurement. The corresponding conductance dip values, $\Delta G/G_\Sigma$, are collected into the third row. The forth row shows the values of (measured) half–widths after the weak tunneling correction, Eq. (93), has been taken into account:

$$V_{1/2,\text{corr.}} \simeq V_{1/2,\text{meas.}}\left[1 - 0.392\frac{\Delta G}{G_\Sigma}\right]. \tag{109}$$

In the fifth row, $\Delta V_{1/2,0}^{\text{corr.}} \equiv (V_{1/2,\text{corr.}} - V_{1/2,0})/V_{1/2,0}$ designates the relative deviations of the corrected half–widths from that of the basic linear relation for $V_{1/2,0}$. The numbers in this row stand for the "residual inaccuracies" of the measured half–widths as compared to the corrections of the weak tunneling approximation. One may expect that these numbers should be due to the strong tunneling effects. The strong tunneling corrections to the half–widths, Eqs. (106) and (107), collected into the last row of Table II, confirm this assumption.

R_T (kΩ)	20	2.1	2.1	1.4	1.0
$V_{1/2,\mathrm{meas.}}$ (mV)	40.20	41.90	41.32	42.22	41.91
$\Delta G/G_\Sigma(\%)$	2.15	2.32	2.26	2.21	1.79
$V_{1/2,\mathrm{corr.}}$ (mV)	39.85	41.52	40.96	41.86	41.62
$\Delta V_{1/2}^{\mathrm{corr.}}/V_{1/2,0}(\%)$	0.5	4.7	3.3	5.6	5.0
$\Delta V_{1/2}^{\mathrm{theor.}}/V_{1/2,0}(\%)$	0.3	3.2	3.2	4.8	5.3

TABLE II: Data for different samples at $T \simeq 4.2$ K. Samples with $R_T = 2.1$ kΩ were further measured at lower temperatures (Fig. 18). The fifth row shows the relative deviations of the half-widths of the basic linear relation, $V_{1/2,0} = 5.439Nk_BT/e$, after the weak tunneling corrections, Eq. (93), have been taken into account. The last row is the prediction of the quasiclassical model [Eqs. (106) and (107)].

3.3.3 Two-dimensional Arrays of Tunnel Junctions

In addition to the one–dimensional (1D) arrays of junctions, two–dimensional (2D) arrays with different number of junctions, island lengths, and various geometries were investigated. The main emphasis was on the use of such structures in thermometric applications and comparison of the results to those of the conventional 1D arrays used as CBT thermometers [38]. Figure 19 shows the schematic of fabricated samples. The bias voltage was applied between the left and the right "busbars" (the vertical bars at the ends). By two–dimensionality, here, we mean that the *islands* between different arrays are connected to each other; *e.g.* Fig. 19 (a) is still a 1D array, whereas Figs. 19 (b) and (c) present 2D structures, where neighboring islands have been interconnected by tunnel junctions.

Samples were made by electron beam lithography and two–angle evaporation techniques. The area of junctions was nominally 0.2×0.6 μm^2. Island sizes, *i.e.* the lengths of the conductors, were varied from 1 μm up to 10 μm. All measurements were carried out at $T = 4.25$ K. To interpret the measured data, the $P(E)$ theory was utilized. In all of the theoretical calculations, the tunneling processes were supposed to be sequential. This is a fairly well–justified assumption: since the per-junction resistances are rather high ($\gtrsim$15 kΩ), one may expect that the probability of cotunneling events is rather small. To characterize

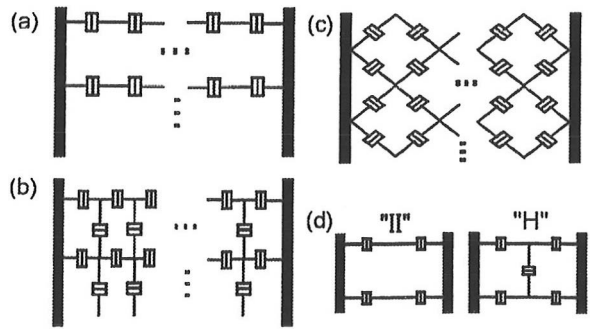

FIG. 19: Schematics of the different one– and two–dimensional (1D and 2D) arrays investigated: **(a)** 1D, **(b)** aligned 2D, **(c)** diagonal 2D, and **(d)** the double junction **II** (left) and the coupled double junction **H** (right) structures.

each kind of the arrays, we use two numbers. N is the number of junctions in a 1D array, and M designates the number of nominally identical arrays in parallel in a 1D structure [Fig. 19 (a)], or in an *aligned* 2D array [Fig. 19 (b)]. In the case of a *diagonal* 2D structure [Fig. 19 (c)], M' stands for the number of nodes at each busbar.

Let us start our study of one– and two–dimensional structures with the simplest arrays with $N = 2$ and $M = 2$ shown in Fig. 19 (d). We denote the corresponding 1D structure by **II** and the 2D structure by **H**, respectively. Figure 20 shows the measured conductance curves of a **II** array (solid line) and an **H** array (dashed line) fabricated simultaneously on the same chip. In both the cases, nominal areas of the tunnel junctions were the same, and the depths of conductance curves, too, were equal, $\Delta G_{\rm T}/G \simeq 0.01$. According to Eq. (93), one expects equal, very small, corrections to the basic half–width relation, Eq. (90), for *both* kinds of the arrays. The simple linear relation, $V_{1/2,0} \simeq 5.439 N k_{\rm B} T/e$, predicts $V_{1/2,0} = 4.0$ mV at $T = 4.25$ K. The measured values, however, are much larger: $V_{1/2} = 4.53 \pm 0.02$ mV and $V_{1/2} = 4.79 \pm 0.05$ mV for **II** and **H** structures, respectively. It should be stressed that this feature is not specific to these samples, and, within the errors given above, it is typical for the rest of the samples, too. (All together, we measured four **II** and seven **H** structures.) This already suggests that Eqs. (90)–(93), derived for the zero–impedance electromagnetic environment, are not sufficient to describe the widening of the half–widths.

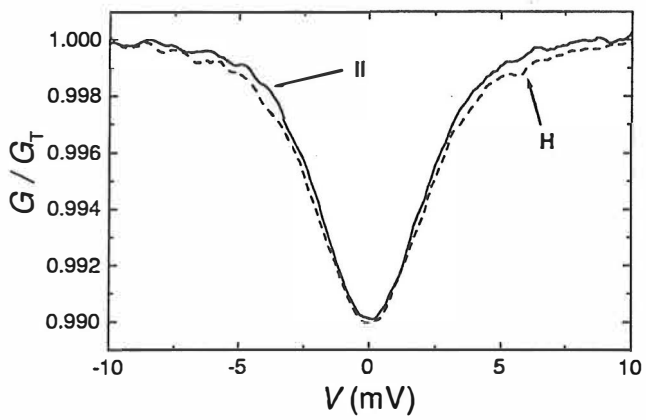

FIG. 20: Measured normalized conductance, $G/G_{\rm T}$, versus bias voltage for the structures **II** (solid line) and **H** (dashed line) of Fig. 19.

However, the half–width of the conductance curve in a 1D array broadens as a consequence of the electromagnetic environment (see Fig. 14) and it has a maximum around the value of free space impedance $Z_0 \simeq 300\ \Omega$. Before going further, let us examine whether this is a general feature for larger structures as well.

Several samples of different sizes and geometries with $N = 8$ were measured. The number of parallel connections was $M = 9$ in 1D, and in aligned 2D arrays. The diagonal 2D structures had $M' = 4$. Figure 21 shows measured conductance curves for 1D (solid line) and for 2D aligned (dashed line) structures. For these samples, too, the depth is still rather small ($\Delta G/G_{\rm T} \sim 0.01$) and, from Eq. (93), one expects a very small correction to the measured half–widths of the samples. However, once again, this is not the case. For 1D arrays, the measured half–widths with $V_{1/2} = 16.68 \pm 0.04$ mV showed a 4 % increase over $V_{1/2,0} = 16.0$ mV . The aligned 2D with $V_{1/2} = 18.20 \pm 0.14$ mV showed a 14 % increase from $V_{1/2,0}$, while corresponding broadening for the diagonal structures with $V_{1/2} = 19.0 \pm 0.27$ mV was even larger, *i.e.* 19 %. Figure 22 shows a histogram of the measured $V_{1/2}$ for these samples together with the prediction of Eq. (90) for $N = 8$ and at $T = 4.2$ K. Figure 23 depicts the dependence of the normalized half-widths, $V_{1/2}/V_{1/2,0}$, of 1D arrays (solid circles)

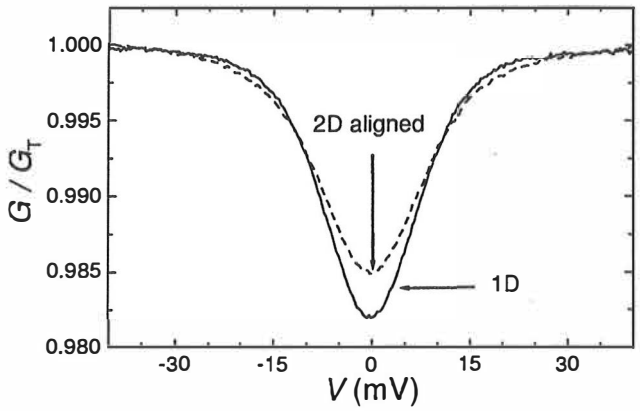

FIG. 21: Measured normalized conductance, $G/G_{\rm T}$, versus bias voltage for the topologies (a) (solid line) and (b) (dashed line) of Fig. 19 with $N = 8$ and $M = 9$ at 4.25 K.

and aligned 2D arrays (solid triangles) on N. The cross in the figure stands for a diagonal 2D array with $N = 8$ and $M' = 4$. Clearly, in the case of 1D arrays the measured half-widths approach $V_{1/2,0}$ more quickly than is the case for 2D arrays. Indeed, from this point of view, these data demonstrate that for small charging peaks ($\Delta G/G_{\rm T} \sim 1\%$), 1D arrays are superior to 2D structures, if one compares them in view of thermometry applications. We also measured few additional arrays with smaller junctions and noticed smaller deviation of $V_{1/2}$ from $V_{1/2,0}$ for these samples. One possible explanation for this can be due to larger junction resistances in arrays composed of smaller junction areas. However, measurements with structures made of small tunnel junctions were not done systematically enough to allow a quantitative conclusion. The broader half–widths in 2D structures cannot be explained within the simple orthodox theory [3] which does not take the effect of electromagnetic environment into account. In this model, the conductance curve can be derived either analytically for 1D arrays in high temperature regime with $u_N \ll 1$ [18], or by Monte–Carlo simulations [8]. In both the cases the conductance curve has the form given by Eq. (89). According to the orthodox theory (or the $P(E)$ theory with negligible environmental impedance), the only difference between the two arrays is the capacitance seen from one

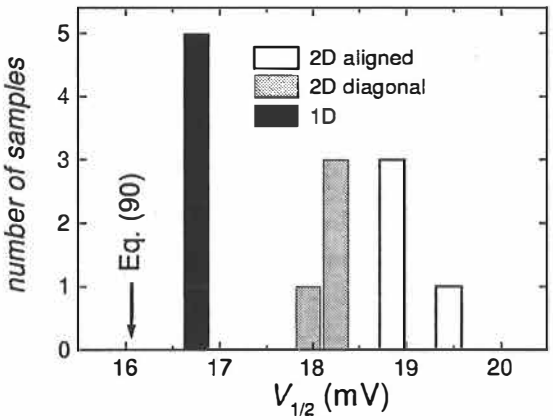

FIG. 22: Histogram of the measured $V_{1/2}$ for the samples with $N = 8$, at $T = 4.25$ K. The filled black bars stand for 1D arrays, the gray bars for diagonal 2D arrays ($M' = 4$), and the open ones for the aligned 2D structures (M=9). The arrow is the value predicted by Eq. (90) with $N = 8$ and $T = 4.2$ K.

of the islands in these structures. For **II** array this capacitance is equal to $2C$, whereas for **H** structure it is $8C/3$. Now, if the orthodox model is valid, one would expect that the depth of the conductance dip, $\Delta G/G_{\rm T}$, in a **II** array should be larger than that of **H** structure by a factor 4/3. The same argument can be generalized to the larger arrays, as well. However, as already noticed, the arrays had the same depths. Therefore, to explain the observed data, one should go beyond the orthodox theory and look for possible improvements by, *e.g.*, taking the environmental or higher order tunneling effects into account. Since the junction resistances are relatively large (15–50 kΩ), the cotunneling events have little chance to happen and, in addition to this, the measured data did not show any correlation with the junction resistances. Assuming the sequential tunneling regime, theoretical description of the 2D structures can be compared to the treatment of one–dimensional arrays already discussed in the previous sections. The only difference, here, is to evaluate the equivalent electromagnetic impedance seen by the junction in which the tunneling event takes place. This is not a straightforward task and, in practice, one should restrict to arrays with a

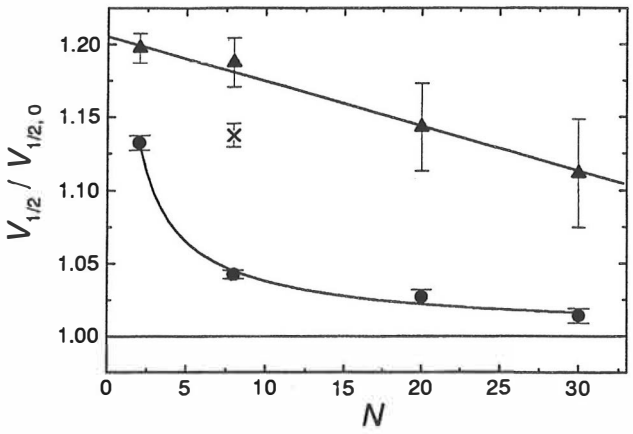

FIG. 23: The normalized measured half–width against number of junctions, N, for 1D (circles) and aligned 2D (triangles) arrays. The solid lines are guides for eye.

smaller number of tunnel junctions. Furthermore, the Monte–Carlo calculations needed in larger 2D arrays become enormously time–consuming, for, generally speaking, the impedance seen by each junction in the structure is different. This means that each tunneling event of simulation has to be performed for a *different* environmental impedance, after which one can proceed to the next steps in the simulation procedure.

To evaluate the tunneling rates of different junctions, we first notice that the impedance of the environment can be decomposed into two parts: the (external) impedance "outside" the array, and the environmental contribution from the array itself. In fact, in some of our former studies [37, 39], we intentionally evaporated thin chromium films onto neighborhood of tunnel junction structures. Here, instead, we mainly consider the internal impedance of the array. To this end, the total environment seen by the k-th junction, $\mathrm{Re}[Z_t^k(\omega)]$, can be supposed as composed of the resistive part R_e connected in series to the terminations of the array (inset of Fig. 24), and the part arising from the capacitances of the surrounding junctions. The resistive part can be supposed to be of the order of free space impedance $\sim 100\ \Omega$ (see, *e.g.*, [P3]). The total impedance $Z_t^k(\omega)$ can now be obtained as the equivalent impedance of the surrounding circuit as seen by the k-th junction. After a straightforward

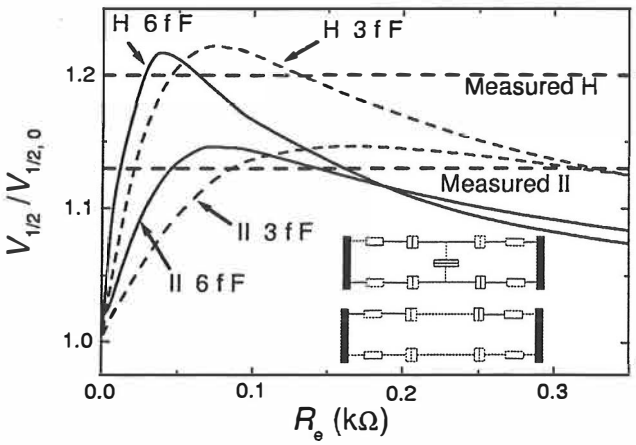

FIG. 24: The circuit models used in calculations (inset), and the theoretically obtained half–widths for the two structures **II** and **H** as functions of external resistive impedance R_e. In all the cases $T = 4.24$ K and all the junctions are identical to $C = 6$ fF (solid line) and $C = 3$ fF (dashed line). Changing either C or T simply scales the values on the horizontal axis; the main parameter in the calculations is $[\hbar/(R_eC)]/(k_BT)$.

calculation for **II** and **H** structures, one gets

$$\mathrm{Re}[Z_t^k(\omega)] = \frac{R_e}{2}\frac{1}{1+(\omega/\omega_c)^2} \tag{110}$$

for all the four junctions in a homogeneous **II** array. Correspondingly, for symmetrically positioned four junctions in an **H** structure, one obtains

$$\mathrm{Re}[Z_t^k(\omega)] = \frac{9R_e}{16}\frac{1+(1/3)(\omega/\omega_c)^2}{1+(5/4)(\omega/\omega_c)^2+(1/4)(\omega/\omega_c)^4}, \tag{111}$$

whereas, for the interconnecting junction

$$\mathrm{Re}[Z_t(\omega)] = \frac{R_e}{4}\frac{1}{1+(1/4)(\omega/\omega_c)^2}. \tag{112}$$

Figure 24 shows the calculated normalized half–width ($V_{1/2}/V_{1/2,0}$, with $N = 2$) against different values of R_e at $T = 4.25$ K. In calculations, we first obtained the IV characteristics for junction capacitances $C = 6$ fF (solid line) and $C = 3$ fF (dashed line). These are values close to the capacitances of our typical samples. Also, in the figure, are shown the

corresponding measured values of $V_{1/2}$. Apparently, the theoretical curves are reminiscent of those obtained for 1D arrays (Fig. 14). In all the cases, the theoretical half–width gets its largest value somewhere in the vicinity of $Z_0 \sim 100\ \Omega$. For these arrays too, the exact position of the maximum of $V_{1/2}$ depends on the (inverse) product of the environmental resistance R_e and the capacitance of the junctions C, *i.e* on ω_c. The magnitude of this maximum, $V_{1/2,max}$, however, seems to be solely dependent on the array geometry. It is systematically larger for **H** array than it is for the **II** and, irrespective of the value of ω_c, it is the same for each type of arrays: $V_{1/2,max} = 4.9$ mV for **H** and $V_{1/2,max} = 4.6$ mV for **II**. These values are in good agreement with those of the measured ones ($V_{1/2} = 4.79 \pm 0.05$ mV for **H**, and $V_{1/2} = 4.53 \pm 0.02$ mV for **II**). Of course, such a good consistency can be achieved, only if we suppose that the "unintentional" on–chip resistances, R_e, are of the order of free space resistance Z_0. This, however, is a rather good conjecture. Other noticeable point in the theoretical curves is that arrays with larger C are more sensitive to the (variations) in R_e: the larger the capacitance, the narrower the maximum against R_e. This explains the larger scatter in the measured data of **H** structures in comparison to those of **II** arrays (see Fig. 23).

In summary, 2D arrays show larger deviation from the predictions of the basic orthodox theory than their 1D counterparts do. Besides this, 2D arrays are more sensitive to the (variations of) electromagnetic environment than their 1D counterparts. This means that, from the thermometric point of view, based on the influence of the electromagnetic environment, 1D arrays are superior to the 2D ones suggested in [38]. However, in both the cases, the effect of environment can be made arbitrarily small by increasing the "size" of the array.

Appendix:

EXPERIMENTAL TECHNIQUES

A.1 Sample Fabrication

Samples were made by electron beam lithography and shadow evaporation techniques. As substrate we have used oxidized (or nitridized) silicon wafers. The reason for this is that plain silicon is a semiconductor and its electrical properties depend on voltage, light, orientation *etc.*, thus affecting the measured electrical quantities of the sample made on it. The thickness of the oxide layer is typically about 300 nm.

As the *resist* layer, *i.e.* the layer onto which the electron beam of the scanning electron microscope (SEM) is directed, we have used PMMA–based solutions. A suitable copolymer resist liquid can be obtained by adding a 9% (weight percentage) of PMMA/MMA into acetic acid. The resist layer on the oxidized wafer can then be formed by dripping a few drops onto the wafer and spinning at the proper speed. Knowing the relation between the speed of spinning and the thickness of the resist, the desired thickness can be obtained. For example, to obtain a $\sim$ 500 nm thick 9% copolymer resist, the proper speed is about 3500 rpm. Usually, we have used a two layer resist structure. As the second (top) layer, we have used a 2–3 % PMMA solution in chlorobenzene. This layer has a smaller thickness, typically $\sim$ 250 nm, and it is made on the first layer and followed by baking it (the first layer) for about 15–30 minutes. This layer too should be baked for a similar period of time on a hot plate with a temperature of about 170 °C. The bottom layer is of higher *sensitivity*.

The next stage is *patterning* of the desired structure onto the resist layer by electron beam lithography. The beam current has been in the range of $\sim$ 20 pA for the fine structures, *i.e.*

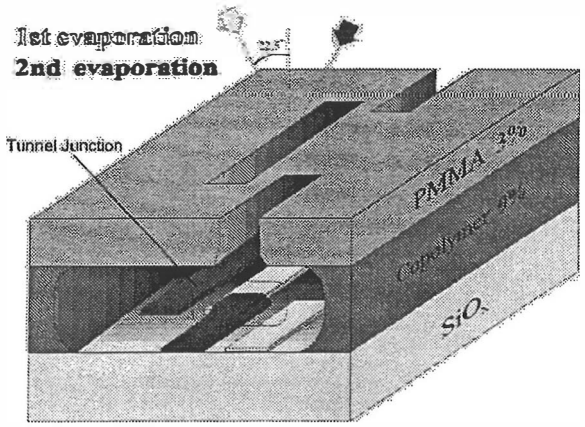

FIG. 25: Schematic view of a sample made by the shadow evaporation technique.

for line-widths in the submicrometer scale, and $\sim$ 50 nA for lines with widths of about few micrometers, or wider.

After the patterns have been drawn onto the resist layer, they should be *developed*. Typically we have used two developers, first of which affects the top layer and the second one the bottom layer more strongly. Developing times were about 30 and 15 seconds in the first and the second developers, respectively. The first developer was a mixture of toluene and isopropanol (volume ratio 1:3) and the second one of ECA and ethanol (1:5).

The pattern on the resist has already been formed, thus making the *mask* structure needed in the next step —the *vacuum evaporation* of films. The exposed wafer is inserted into a vacuum chamber, and after reaching a good vacuum (typically $< 10^{-5}$ mbar) the evaporation of the desired material can be started. In our experiments, to form the tunnel junctions, we have used aluminum (Al). To realize the dissipative electromagnetic environment in the vicinity of tunnel junctions, one should use a material with high resistivity. A good choice is chromium (Cr). In the evaporator the beam of electrons radiated from a filament (with a voltage difference of about 40 kV across) is focused by a magnetic field. The *evaporation rate* for aluminum films was about 5–10 Å/s and for chromium somewhat smaller, 2–5 Å/s. Typically, we have made Cr–films with resistances of about few kilo-ohms. The thickness of evaporated film is evaluated by a quartz crystal. The material evaporated changes the

mass of the crystal, thus changing its resonance frequency. Measuring this frequency, one can estimate the thickness. Figure 25 demonstrates the stages described. After the vacuum evaporation, the resist layer is washed out in acetone. This is called *lift–off* process. Now the sample is ready for measurement.

A.2 Cooling of the Samples

Some of the measurements, like those in [P3] and [P4], were performed only at liquid helium temperature, $T \simeq 4.2$ K. Some others were performed at temperatures from $T \simeq 4.2$ K down to $T \simeq 1.5$ K ([P5]), and there were also measurements in the millikelvin range, down to $T \simeq 30$ mK ([P1] and [P2]). The "dipstick measurement" in liquid helium is the simplest, and one does not need any particular cool–down procedure.

To perform measurements at lower temperatures, we have used a home–made *plastic* ^{3}He–^{4}He dilution refrigerator [41]. Temperatures down to 30 mK can be reached by this instrument. The "physics" of dilution refrigeration is well understood and can be found in many textbooks, *e.g.* in [42]. To measure the temperature, we used the liquid helium vapor pressure data, calibrated resistance thermometers, and Coulomb blockade thermometers (CBT sensors) developed in our laboratory [18].

A.3 Measuring Electronics

Two key points in measuring differential conductance (or resistance) of the samples used here (and in other precise measurements) are the *four–wire measurement* and the *lock–in* techniques.

The idea in four–wire measurement is to suppress the influence of *lead* resistances. In a conventional two–wire measurement, a test current is passed through the component to be measured, *e.g.* a resistance, and the voltage drop across the component is measured by a voltmeter. If the lead resistances are negligible in comparison to the resistance to be measured, this method is precise enough, otherwise one has either to know the lead resistances or, even better, to use the four–wire technique. In the four–wire configuration,

the current through the sample and the voltage across it are measured through different probes.

Generally, the lock–in techniques are used for three reasons: to improve the signal to noise ratio, to measure the phase difference between two signals, and to subtract the static bias, like the thermo–voltage. That is why, whatever the final goal is, one has to have *ac* signals at frequency ν in the input of the measurement system. What lock–in amplifier does, is to distinguish signals of *reference frequency* ν in the output. In this respect it is very similar to a filter with a very high quality factor ($\sim 10^6$). Furthermore, it is an amplifier. In a lock–in amplifier, the output signal is proportional to the product of amplitudes of the input and the reference signals, and its magnitude is a trigonometric function of the phase difference between these signals. That is why during the measurement, one tries to adjust the "phase" in such a way that the output signal is as large as possible. While using lock–in techniques, one should take care about the magnitude of the *ac* signal superimposed on the original signal. The amplitude of the auxiliary signal is to be as small as possible with still sufficient signal to measure. Besides this, the frequencies of auxiliary and reference signals should be chosen small to reduce the effect of reactive components of the impedance but not too small to avoid low frequency noise (*e.g.* $1/f$ noise) [33]. Typical values in our measurements have been $\sim$10 Hz for frequency, $\sim$20 mV for the (rms) *ac* voltage, and $\sim$ 1 s for the time constant of the lock–in amplifier. The value of the *biasing resistor* $R_{\rm bias}$ depends on the magnitude of the asymptotic tunnel resistance $R_{\rm T}$, *e.g.*, for a single tunnel junction with $R_{\rm T} \simeq 100$ kΩ, the suitable choice for $R_{\rm bias}$ could be $\sim$10 MΩ. If possible, it is better not to use very large values of $R_{\rm bias}$, because large resistances impose larger (thermal) noise on the signal. Typical value for gains in the pre–amplification of signals has been 50. To carry signals between the sample holder in the cryostat and the measuring setup at room temperature, twisted manganin wires were used, because of their low thermal conductivity and small temperature dependence of resistivity. In the very vicinity of the sample, we used thermo–coax cables and silver wire. Wire contacts to the sample were indium soldered. To confirm the reliability and reproducibility of the measurements, we have used different values of, *e.g.*, excitation and reference signals, biasing resistors, and in some occasions, filters, and

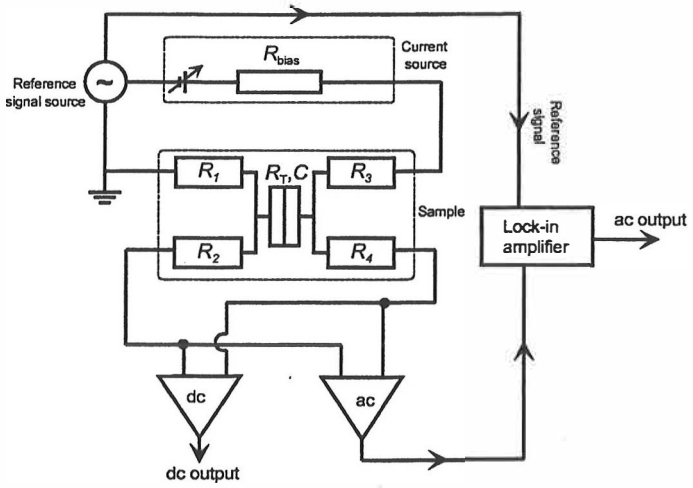

FIG. 26: Schematic of the setup used in a differential resistance measurement. The *dc* output gives the (sweep) bias voltage V, whereas the *ac* output is proportional to the differential resistance, $\mathrm{d}V/\mathrm{d}I$, of the sample.

performed the measurements for, at least, a few times. All the measuring facility, except the data collecting computer, have been kept in the shielded room to reduce pick-up. For example, we have noticed that the operating mobile phones can disturb the measurement noticeably. Figure 26 shows the setup used in a typical differential resistance measurement.

REFERENCES

[1] M. Tinkham, Am. J. Phys. **64**, 343 (1996).

[2] T. A. Fulton and G. J. Dolan, Phys. Rev. Lett. **59**, 109 (1987).

[3] D. V. Averin and K. K. Likharev, Ch. 6 in *Mesoscopic Phenomena in Solids*, edited by B. L. Altshuler, P. A. Lee, and R. A. Webb (Elsevier, Amsterdam, 1991).

[4] A. O. Caldeira and A. J. Leggett, Ann. Phys. (N.Y.) **149**, 374 (1983).

[5] M. H. Devoret, D. Esteve, H. Grabert, G.-L. Ingold, H. Pothier, and C. Urbina, Phys. Rev. Lett. **64**, 1824 (1990).

[6] G.-L. Ingold and Yu. V. Nazarov, Ch. 2 in *Single Charge Tunneling*, Vol. 294 of NATO Advanced Study Institute Series B, edited by H. Grabert and M. H. Devoret (Plenum, New York, 1992).

[7] H. Grabert, G.-L. Ingold, M. H. Devoret, D. Esteve, H. Pothier, and C. Urbina, Z. Phys. B **84**, 143 (1991).

[8] K. P. Hirvi, M. A. Paalanen, and J. P. Pekola, J. Appl. Phys. **80**, 256 (1996); K. P. Hirvi, Ph.D. thesis, University of Jyväskylä (1997).

[9] A. N. Korotkov (private communication).

[10] N. S. Bakhvalov, G. S. Kazacha, K. K. Likharev, and S. I. Serdyukova, Sov. Phys. JETP **68**, 581 (1989).

[11] P. Joyez, D. Esteve, and M. H. Devoret, Phys. Rev. Lett. **80**, 1956 (1998).

[12] A. A. Odintsov, Sov. Phys. JETP **67**, 1265 (1988); A. A. Odintsov, Sov. J. Low Temp. Phys. **15**, 263 (1989).

[13] R. P. Feynman, R. B. Leighton, and M. Sands, *The Feynman Lectures on Physics* (Addison Wesley, Reading, 2nd printing, 1966).

[14] G. Göppert, X. H. Wang and H. Grabert, Phys. Rev. B **55**, R10213 (1997) ; X. H. Wang and K. A. Chao, Phys. Rev. B **56**, 12404 (1997).

[15] J. J. Toppari, M.Sc. thesis, University of Jyväskylä (1997).

[16] See, *e.g.*, M. R. Spiegel, Mathematical Handbook of Formulas and Tables (McGraw–Hill, 30th printing, 1992).

[17] P. Joyez and D. Esteve, Phys. Rev. B **56**, 1848 (1997).

[18] J. P. Pekola, K. P. Hirvi, J. P. Kauppinen, and M. A. Paalanen, Phys. Rev. Lett. **73**, 2903 (1994); Sh. Farhangfar, K. P. Hirvi, J. P. Kauppinen, J. P. Pekola, J. J. Toppari, D. V. Averin, and A. N. Korotkov, J. Low Temp. Phys. **108**, 191 (1997).

[19] U. Eckern, G. Schön, and V. Ambegaokar, Phys. Rev. B **30**, 6419 (1984).

[20] G. Schön, Phys. Rev. B **32**, 4469 (1985).

[21] H. B. Callen and T. A. Welton, Phys. Rev. **83**, 34 (1951). A thorough discussion of the fluctuations (and dissipations) is given by L. D. Landau and E. M. Lifshitz in *Statistical Physics, Part I* (Pergamon Press, 3rd edition, 1985).

[22] R. H. Koch, D. J. van Harlingen, and J. Clarke, Phys. Rev. Lett. **45**, 2132 (1980).

[23] A. Schmid, J. Low Temp. Phys. **149**, 609 (1982).

[24] A. J. Dahm, A. Denenstein, D. N. Langenberg, W. H. Parker, D. Rogovin, and D. J. Scalapino, Phys. Rev. Lett. **22**, 1416 (1966).

[25] E. Ben-Jacob, D. J. Bergman, B. J. Matkowsky, and Z. Schuss, Phys. Lett. A **99**, 343 (1983).

[26] D.S. Golubev and A.D. Zaikin, Phys. Rev. B **46**, 10903 (1992). A similar approach based on the analogy with the polaron problem was developed by A.A. Odintsov, Zh. Eksp. Teor. Fiz. **94**, 312 (1988) [Sov. Phys. JETP, **67**, 1265 (1988)].

[27] D.S. Golubev and A.D. Zaikin, Phys. Lett. **A169**, 475 (1992).

[28] D.S. Golubev and A.D. Zaikin, Zh. Eksp. Teor. Fiz. Pis'ma Red. **63**, 953 (1996) [JETP Letters **63**, 1007 (1996)].

[29] D.S. Golubev, J. König, H. Schoeller, G. Schön and A.D. Zaikin. Phys. Rev. B **56**, 15782 (1997).

[30] Sh. Farhangfar, R. S. Poikolainen, J. P. Pekola, D. S. Golubev and A. D. Zaikin, to appear in Phys. Rev. B (Feb. 15, 2001) [cond-mat/0005283].

[31] J. König, H. Schoeller, and G. Schön, Phys. Rev. B **58**, 7882 (1998).

[32] A. N. Cleland, J. M. Schmidt and J. Clarke, Phys. Rev. Lett. **64**, 1561 (1990); A. N. Cleland, A. N. Schmidt and J. Clarke, Phys. Rev. B **45** 2950 (1992).

[33] Sh. Kogan, *Electronic Noise and Fluctuations in Solids* (Cambridge University Press,

Cambridge, 1996).

[34] K. P. Hirvi, J. P. Kauppinen, A. N. Korotkov, M. A. Paalanen, and J. P. Pekola, Appl. Phys. Lett. **67**, 2096 (1995).

[35] J. P. Kauppinen and J. P. Pekola, Phys. Rev. B **54**, R8353 (1996).

[36] J. P. Kauppinen, Ph.D. thesis, University of Jyväskylä (1998).

[37] Sh. Farhangfar, J. J. Toppari, Yu. A. Pashkin, A. J. Manninen and J. P. Pekola, Europhys. Lett. **43**, 59 (1998).

[38] T. Bergsten, T. Claeson, and P. Delsing, J. Appl. Phys. **86**, 3844 (1999).

[39] Sh. Farhangfar, A. J. Manninen, and J. P. Pekola, Europhys. Lett **49**, 237 (2000).

[40] J. P. Pekola, L. J. Taskinen, and Sh. Farhangfar, Appl. Phys. Lett. **76**, 3747 (2000).

[41] J. P. Pekola and J. P. Kauppinen, Cryogenics **34**, 843 (1994).

[42] F. Pobell, *Matter and Methods at Low Temperatures* (Springer Verlag, Berlin and Heidelberg, 2nd edition, 1996).